https://doi.org/10.5194/egusphere-2026-513
Preprint. Discussion started: 23 March 2026

Impacts of land-use and land-cover change on blue–green water partitioning

Simon P. Heselschwerdt[1,2], Abhinav Dengri[1], Nora L. S. Fahrenbach[3], and Peter Greve[1]

[1]Climate Service Center Germany (GERICS), Helmholtz-Zentrum Hereon, Hamburg, Germany
[2]Institute of Environmental Science and Geography, University of Potsdam, Potsdam, Germany
[3]Institute for Atmospheric and Climate Science, ETH Zurich, Zurich, Switzerland

Correspondence: Simon P. Heselschwerdt (simon.heselschwerdt@hereon.de)

Abstract. Land-use and land-cover change (LULCC) is a major driver of terrestrial water cycle changes, yet its effects on how precipitation is partitioned into blue (runoff) and green water (transpiration) flows remain unclear. Here we address this knowledge gap using Earth system model simulations from the Land Use Model Intercomparison Project (LUMIP) under contrasting socioeconomic pathways (SSP1-2.6 and SSP3-7.0). We find that future sustainable LULCC (i.e., predominantly avoided deforestation and preservation of natural non-forest ecosystems) significantly impacts blue–green water partitioning, with regions showing positive leaf area index (LAI) and gross primary productivity (GPP) responses generally corresponding to larger green water shares. These effects are strongest in the tropics and particularly during dry seasons, where LAI and GPP responses are largest. Regions with the strongest green water gains show the highest sensitivity of blue–green water partitioning to vegetation responses, with the largest partitioning shifts per unit change in LAI or GPP. Precipitation responses to LULCC further modulate the strength of blue–green water partitioning shifts. In some regions, higher transpiration is partly offset by increased rainfall, limiting reductions in blue water availability. While we find consistent ecohydrological responses to LULCC across the multi-model ensemble mean, substantial regional inter-model disagreement arises due to differences in model-specific plant functional types and their parametrisations. Our results underscore that the water cost or benefit of land management depends jointly on vegetation function, precipitation feedbacks, and model structural uncertainty.

1 Introduction

Land-use and land-cover change (LULCC) is a central driver of Earth system functioning, shaping the coupled carbon, energy, and water cycles (Bonan, 2008; Lawrence et al., 2016; Pongratz et al., 2021). These impacts arise from both biogeochemical effects (including changes in carbon storage and CO_2 fluxes) and biogeophysical effects (including albedo, aerodynamic roughness, and evapotranspiration). Beyond its contribution to the global carbon budget (Friedlingstein et al., 2023), LULCC directly influences terrestrial hydrology by altering the partitioning of precipitation between evapotranspiration, storage, and runoff, and by modifying land–atmosphere interactions that can feed back on precipitation (Lawrence et al., 2016; Pongratz et al., 2021). These interactions are increasingly policy-relevant because land-based mitigation and carbon-dioxide removal options, including afforestation, avoided deforestation, and bioenergy crops, are often evaluated primarily for their carbon benefits despite potentially far-reaching consequences for water availability (Pongratz et al., 2021). In many settings, increasing

https://doi.org/10.5194/egusphere-2026-513
Preprint. Discussion started: 23 March 2026

tree cover enhances evapotranspiration and can affect precipitation, which may reduce downstream water availability and intensify competition for water resources (Asselin et al., 2024; Jackson et al., 2005; Ricciardi et al., 2022). Quantifying how sustainable LULCC shifts precipitation partitioning is therefore essential to assess trade-offs and co-benefits across climate mitigation, ecosystem functioning, and water security.

The water-cycle consequences of LULCC can be addressed from a blue–green water perspective, which distinguishes blue water in rivers, lakes, reservoirs, and aquifers that is directly accessible for human use from green water stored as soil moisture in the unsaturated root zone that sustains vegetation and returns to the atmosphere as vapour (Falkenmark, 1995; Falkenmark and Rockström, 2006; Gleeson et al., 2020; Rockström and Gordon, 2001). In Earth system models (ESMs), these two resources are most consistently assessed through their associated flows, because blue water storage is not represented in a harmonised way across land model components. We therefore characterise blue–green partitioning using runoff as a proxy for the blue water flow and transpiration as the (productive) green water flow, consistent with the blue–green water framework and its applications in global model analyses (Falkenmark and Rockström, 2006; Orth and Destouni, 2018; Hoekstra, 2019). To quantify this partitioning, we use the Blue–Green Water Share (BGWS; Heselschwerdt et al., 2025), a process-based metric that diagnoses how an incremental unit of precipitation is allocated between blue (runoff) and green water flow (transpiration) (Sect. 2.3). Here, we focus on transpiration rather than total evapotranspiration because transpiration directly reflects vegetation water use, whereas evapotranspiration also includes soil evaporation that can vary independently of vegetation functioning (Rockström and Gordon, 2001; Falkenmark and Rockström, 2006).

Precipitation responses to LULCC are a key, yet still uncertain, link between land management and blue–green water partitioning. LULCC can influence precipitation through changes in evapotranspiration and terrestrial moisture recycling as well as through circulation adjustments and related changes in moisture convergence driven by altered surface roughness and energy partitioning. Because a substantial share of land precipitation originates from upwind land evapotranspiration, rainfall responses can propagate along precipitationsheds and depend on where land-use change occurs relative to key moisture-source regions (van der Ent et al., 2010; Tuinenburg et al., 2020; te Wierik et al., 2021). In the tropics, forest loss has been linked to regional drying and increased water stress, while the magnitude and even the sign of rainfall responses can vary with season and with the location of land-cover change relative to upwind moisture sources (Spracklen et al., 2012; Staal et al., 2018; Wang-Erlandsson et al., 2018). Beyond these recycling-driven effects, LULCC can also perturb the surface energy budget and shift large-scale circulation, including the Hadley cell and the Intertropical Convergence Zone (ITCZ). This can generate remote precipitation changes far from the land-use perturbation (Swann et al., 2012; Devaraju et al., 2015; Laguë and Swann, 2016; Portmann et al., 2022).

Reflecting the interplay of multiple, sometimes opposing mechanisms, coupled-model analyses of future land-based mitigation pathways and forestation scenarios often find that increasing tree cover raises evapotranspiration and can increase precipitation, yet still reduces water availability (P−ET) in parts of the tropics, including regions of Africa (Fahrenbach et al., 2025; King et al., 2024). This reflects a net shift toward higher vegetation water use, where transpiration gains outweigh precipitation increases and can depress runoff. Catchment syntheses similarly report reduced streamflow following afforestation, while global modelling suggests that outcomes remain spatially heterogeneous and depend strongly on background aridity and

https://doi.org/10.5194/egusphere-2026-513
Preprint. Discussion started: 23 March 2026

land–atmosphere feedbacks (Jackson et al., 2005; Farley et al., 2005; Cui et al., 2022). This highlights that assessing hydrological consequences of LULCC requires considering not a single hydroclimate variable in isolation, but the combined effects on precipitation, vegetation water use, and runoff.

Recent regional modelling studies have started to frame LULCC impacts on blue–green water partitioning explicitly and show a redistribution from blue to green fluxes under forest expansion (Asselin et al., 2024). At larger scales, modelling and diagnostic studies further suggest that tree-cover change can modulate runoff in ways that may offset or amplify climate-driven runoff changes, underscoring that land management can be a first-order control on regional blue water resources (Engel et al., 2025). In ESMs, the resulting partitioning response also depends on how land-cover transitions are mapped onto plant functional types (PFTs) and how key ecohydrological processes (e.g., transpiration, interception, and runoff generation) are parametrised (Pitman et al., 2009; Boysen et al., 2020; Egerer et al., 2025). Single-model analyses may therefore be strongly contingent on model-specific biases, vegetation parameter settings, and land-cover mapping strategies. This motivates multi-model assessments that quantify uncertainty ranges and help identify robust ecohydrological responses. Despite extensive work on runoff, evapotranspiration, and water availability responses to LULCC, global assessments that explicitly quantify shifts in blue–green water partitioning and systematically characterise inter-model spread remain scarce.

Here, we use four ESM simulations from the Coupled Model Intercomparison Project phase 6 (CMIP6; Eyring et al., 2016) and its Land Use Model Intercomparison Project (LUMIP; Lawrence et al., 2016) to assess how sustainable LULCC alters the partitioning of precipitation into green water flow (transpiration) and blue water flow (runoff). Using the LUMIP experiment design, we isolate the future sustainable (i.e. avoided deforestation and preservation of natural non-forest ecosystems) LULCC signal (2070–2099) from the background climate change response and diagnose blue–green partitioning using the BGWS metric. Specifically, we ask where and in which seasons sustainable LULCC shift BGWS, whether these shifts are mediated mainly through vegetation water use or through precipitation feedbacks, and how consistent the inferred responses are across models. Resolving these questions can help to clarify how land-based mitigation affects the terrestrial water cycle and frame afforestation and avoided deforestation in the broader context of water security under net-zero pathways.

2 Data and methods

2.1 Experiment design

We quantify LULCC impacts on late-21st-century (2070–2099) blue–green water partitioning using simulations from LUMIP (Lawrence et al., 2016)). We contrast two future Shared Socioeconomic Pathways (SSPs) that differ in socioeconomic development and radiative forcing and, importantly for this study, in land-use trajectories: SSP1-2.6, which features reduced deforestation and net forest-cover gain under strong mitigation (Riahi et al., 2017), and SSP3-7.0, which features substantial cropland expansion and widespread deforestation under high forcing (Fujimori et al., 2017). These scenarios focus on large-scale, multi-decadal land-use transitions rather than local afforestation or conservation projects.

To isolate the LULCC contribution from the background climate and forcing differences between SSPs, we use the LUMIP land-use-swap experiments (Lawrence et al., 2016). In *ssp126-ssp370Lu*, all forcings follow SSP1-2.6 except that land use is

https://doi.org/10.5194/egusphere-2026-513
Preprint. Discussion started: 23 March 2026

prescribed from SSP3-7.0 (denoted L3), while *ssp370-ssp126Lu* follows SSP3-7.0 forcings with SSP1-2.6 land use (denoted L1). Here, *Lu* denotes that only land use is taken from the alternative scenario. These counterfactual combinations are not intended as plausible socio-economic futures, but as a controlled design to separate land-use effects from the rest of the scenario forcing (Lawrence et al., 2016). For brevity, we denote the four simulations as S1L1 (*ssp126*), S3L3 (*ssp370*), S1L3 (*ssp126-ssp370Lu*), and S3L1 (*ssp370-ssp126Lu*).

We diagnose the sustainable LULCC signal (Δ_{LULCC}; Eq. 1) as the symmetric mean of the L1–L3 land-use contrast under low-forcing (S1) and high-forcing (S3) background climates, following Fahrenbach et al. (2025):

$$\Delta_{\mathrm{LULCC}} = \frac{1}{2}\left(\mathrm{S1L1} - \mathrm{S1L3}\right) + \frac{1}{2}\left(\mathrm{S3L1} - \mathrm{S3L3}\right). \tag{1}$$

The resulting Δ_{LULCC} provides a climate-robust estimate of the land-use signal for two reasons: (1) it quantifies LULCC impacts on blue–green water partitioning under distinct background climates, acknowledging that land-use effects on hydrology may depend on the prevailing climate state; and (2) by averaging across both backgrounds, it reduces dependence on which forcing pathway (SSP1-2.6 vs. SSP3-7.0) is used as the climate context and improves the signal-to-noise ratio of the inferred LULCC response.

Notably, the SSP simulations analysed here are concentration-driven. As a result, they capture the biogeophysical impacts of LULCC (and vegetation responses to the prescribed CO_2 pathway), but they do not include the additional climate feedback that would arise if LULCC carbon emissions altered atmospheric CO_2 concentrations (Lawrence et al., 2016; Amali et al., 2025). We therefore interpret Δ_{LULCC} primarily as the biogeophysical land-use imprint on the hydrological cycle under a prescribed background climate trajectory. Because we contrast two future land-use pathways, positive responses in vegetation metrics (e.g., ΔLAI, ΔGPP) indicate higher values relative to the unsustainable land-use pathway (L3) and may reflect avoided or reduced deforestation rather than absolute greening.

For context, we additionally analyse historical LUMIP simulations over 1985–2014 by contrasting historical and *hist-noLu* (fixed 1850 land use) simulations and define the historical LULCC signal as *historical* − *hist-noLu* (Lawrence et al., 2016). This comparison is reported in the Supplementary and is used as supporting evidence rather than a core result.

2.2 ESM data

We use output from four CMIP6 ESMs participating in LUMIP (Table 1). The ESMs were selected based on the availability of monthly output for all experiments described in Sect. 2.1 and for all variables required in our analysis. The core ensemble comprises the Beijing Climate Center Climate System Model version 2 (BCC-CSM2-MR; hereafter BCC-CSM2), the Euro-Mediterranean Centre on Climate Change Earth System Model version 2 (CMCC-ESM2), the Model for Interdisciplinary Research on Climate Earth System version 2 for Long-term simulations (MIROC-ES2L), and the United Kingdom Earth System Model version 1.0 in its low-resolution configuration (UKESM1-0-LL; hereafter UKESM1). Further details on horizontal resolution and land surface configurations are provided in Table 1, while Supplement S1 summarises the representation of relevant ecohydrological processes in the respective land surface models (LSMs).

https://doi.org/10.5194/egusphere-2026-513
Preprint. Discussion started: 23 March 2026

Table 1. Overview of CMIP6 ESMs used in this study, including ensemble members, LSMs, interactive terrestrial nitrogen-cycle representation (N cycle), horizontal resolution, number of PFTs, vegetation dynamics, and primary references.

Model	Ensemble member(s)	LSM	N cycle	Resolution (lat×lon)	PFTs	Vegetation dynamics	Reference
BCC-CSM2-MR	r1i1p1f1	BCC_AVIM2.0	No	∼1.125°× ∼1.125° (T106, Gaussian)	15	Prescribed PFT fractions; prognostic LAI	Wu et al., 2019
CMCC-ESM2	r1i1p1f1	CLM4.5-BGC	Yes	0.9°× 1.25°	15	Prescribed PFT fractions; prognostic phenology/LAI	Lovato et al., 2022
MIROC-ES2L	r1i1p1f2	MATSIRO + VISIT-e	Yes	∼2.8°× ∼2.8° (T42, Gaussian)	12	Prescribed vegetation fractions; prognostic LAI	Hajima et al., 2020
UKESM1-0-LL	r1–r4i1p1f2	JULES-ES-1.0 (TRIFFID)	Yes	1.25°× 1.875°	13	Dynamic PFT competition within natural/managed units	Sellar et al., 2019

We primarily assess 30-year mean responses in total precipitation (P; $\mathrm{mm\,day^{-1}}$), runoff (R; $\mathrm{mm\,day^{-1}}$), transpiration (E_t; $\mathrm{mm\,day^{-1}}$), leaf area index (LAI; $\mathrm{m^2\,m^{-2}}$), and gross primary productivity (GPP; $\mathrm{gC\,m^{-2}\,day^{-1}}$). In addition, we include evapotranspiration (ET; $\mathrm{mm\,day^{-1}}$) and surface soil moisture from the CMIP6 variable *mrsos*, which represents moisture in the upper soil layer (0–10 cm; mm). Evaporation (E; $\mathrm{mm\,day^{-1}}$), including soil evaporation and canopy interception losses, is not available as standard output for all four ESMs. We therefore compute it as the residual

$$E = ET - E_\mathrm{t}. \tag{2}$$

Only UKESM1 provides multiple ensemble members for the required experiments, with four realisations available (Table 1). We therefore analyse the UKESM1 ensemble mean to reduce the influence of internal variability. For the other three ESMs, only a single ensemble member is available, such that the contribution of internal variability differs across models. To enable uniform spatial comparisons between models with different native grids, we conservatively regrid all data to a common 1°× 1° grid.

To document the imposed land-use transitions, we analyse the Land-Use Harmonization dataset version 2 (LUH2) (Hurtt et al., 2020). LUH2 is a harmonised land-use dataset used as external forcing in CMIP6, including the LUMIP simulations, and provides annually varying land-use states and transitions for the SSP scenarios (Lawrence et al., 2016). We aggregate LUH2 state variables into broad land-use categories, including forest (primary plus secondary forest), cropland (annual and perennial crop types), grazing land (pasture plus rangeland), and natural non-forest vegetation, and compute 30-year mean differences for 2070–2099 between SSP1-2.6 and SSP3-7.0 to quantify LULCC differences between the pathways. We additionally compare these future land-use states with the historical reference period (1985–2014) to assess whether scenario differences actually reflect expansion (e.g., afforestation) or reduction (e.g., avoided deforestation) of the land-use type (Fig. S1).

To compare LUH2 forcing fractions with the realised land-cover response within each ESM, we include model land-cover diagnostics where available, specifically tree fraction (*treeFrac*; %) and land-use tile fractions (*fracLut*; %). The latter provides information on primary and secondary natural vegetation, cropland, and pasture fractions. Availability differs across the en-

https://doi.org/10.5194/egusphere-2026-513
Preprint. Discussion started: 23 March 2026

semble: these diagnostics are not available for BCC-CSM2; CMCC-ESM2 provides tree fraction only; MIROC-ES2L provides land-use tile fractions; UKESM1 provides tree fraction for all four ensemble members, while land-use tile fractions are available only for the r4i1p1f2 member. We analyse these land-use state variables as 30-year mean differences where available to assess the correspondence between LUH2 and model-specific land-cover changes (Fig. S2).

Because responses in blue–green water partitioning depend strongly on how each model translates land-use forcing into vegetation function, we prioritise LAI and GPP as diagnostics of the vegetation response. We interpret LAI as an indicator of canopy structure and cover and GPP as an indicator of plant productivity. We therefore relate changes in LAI and GPP to changes in E_t, P, and R throughout the analysis, rather than relying solely on land-cover fractions, which can be mapped differently across ESMs and do not capture functional differences in vegetation response.

In addition to the core four-model ensemble used throughout this study, we include an extended ensemble of five additional CMIP6 ESMs (Table S1) that is available only for the historical period. We use this nine-model ensemble to benchmark the historical LULCC signal of the four-model multi-model mean (MMM). To evaluate whether the four-model MMM is representative, we compare the historical LULCC signal in blue–green water partitioning between the four-model and nine-model MMMs over 1985–2014 (Fig. S4). The resulting spatial patterns show moderate-to-strong agreement (Pearson $r = 0.73$), indicating that the core ensemble captures the main large-scale features of the simulated LULCC response. However, because the four core models are part of the nine-model MMM, this comparison is not fully independent. When comparing the four-model MMM with the MMM of the five additional models only, agreement is weak (Pearson $r = 0.30$), highlighting substantial structural uncertainty in the land-use signal. We therefore interpret the four-model future results as one plausible realisation within a wider range of model responses and explicitly discuss uncertainty across models.

2.3 Blue–Green Water Share

We quantify the relative partitioning of precipitation into blue water (runoff) and green water (transpiration) flows using the Blue–Green Water Share (BGWS) metric introduced in Heselschwerdt et al. (2025). BGWS is a signed, normalised index that expresses the dominance of runoff (R) versus transpiration (E_t) relative to total precipitation (P):

$$\mathrm{BGWS} = \frac{R - E_t}{P} \times 100. \tag{3}$$

We use transpiration (E_t) as the green water flow because it directly represents vegetation water use, whereas evapotranspiration includes non-transpirative components (e.g., soil evaporation and interception losses) that can vary independently of vegetation functioning. Positive BGWS values indicate a greater relative partitioning of precipitation to blue water flow and negative values indicate a greater partitioning to green water flow. Differences between simulations (ΔBGWS) quantify shifts in partitioning. Because BGWS is defined as a ratio, we exclude grid cells with very low hydrological activity to avoid unstable values. We apply a common mask derived from the historical four-model MMM (1985–2014), retaining only grid cells where the 30-year mean fluxes satisfy $\overline{P} > 0.05\,\mathrm{mm\,day^{-1}}$, $\overline{E_t} > 0.005\,\mathrm{mm\,day^{-1}}$, and $\overline{R} > 0.005\,\mathrm{mm\,day^{-1}}$. The same mask is applied to all scenarios, models, and variables to ensure consistent spatial comparability.

https://doi.org/10.5194/egusphere-2026-513
Preprint. Discussion started: 23 March 2026

To summarise the relative magnitude of the LULCC effect on BGWS, we compute a fractional BGWS impact at each land grid cell as the absolute sustainable LULCC signal normalised by the background BGWS state,

$$I_{\mathrm{BGWS}} = 100 \times \frac{|\Delta\mathrm{BGWS}_{\mathrm{sustain\,LULCC}}|}{|\mathrm{BGWS}_{\mathrm{ref}}|}, \tag{4}$$

where $\Delta\mathrm{BGWS}_{\mathrm{sustain\,LULCC}}$ denotes the sustainable LULCC signal (Sect. 2.1) and $\mathrm{BGWS}_{\mathrm{ref}} = \frac{1}{2}\left(\mathrm{BGWS}_{\mathrm{S1L1}} + \mathrm{BGWS}_{\mathrm{S3L3}}\right)$ is the mean BGWS of the two baseline scenario simulations. We summarise I_{BGWS} by the land median.

2.4 Quantile regression analysis

To investigate how vegetation responses to LULCC relate to shifts in blue–green water partitioning, we apply linear quantile regression between ΔBGWS and vegetation responses (ΔLAI, ΔGPP) across the conditional distribution of ΔBGWS. For each predictor $X \in \{\Delta\mathrm{LAI}, \Delta\mathrm{GPP}\}$, we fit

$$Q_\tau(\Delta\mathrm{BGWS} \mid X) = \beta_0(\tau) + \beta_1(\tau)\,X, \quad \tau \in \{0.10, 0.50, 0.90\}. \tag{5}$$

Here, Q_τ denotes the τ-th conditional quantile. In all cases, ΔBGWS is treated as the dependent variable and ΔLAI or ΔGPP as the independent variable, consistent with a process-based direction of effect. Fits are performed across land grid cells for each model and for the MMM, using the LULCC-induced differences defined in Sect. 2.1.

The regression slopes $\beta_1(\tau)$ measure how strongly the τ-th conditional quantile of ΔBGWS changes per unit change in X; negative slopes imply that positive vegetation responses (e.g., higher ΔGPP) are associated with shifts toward green water partitioning (sign convention used here). Comparing $\beta_1(0.10)$, $\beta_1(0.50)$, and $\beta_1(0.90)$ reveals whether sensitivity differs between grid cells exhibiting strong green water share increases (lower tail), median responses, or strong blue water share increases (upper tail) (Koenker and Hallock, 2001).

3 Results

3.1 Vegetation response to sustainable LULCC

Figures 1 and 2 map the vegetation response to sustainable LULCC for the MMM (a) and each individual model (b–e), together with the corresponding zonal means (f). The strongest positive ΔLAI signals ($\geq 0.5\ \mathrm{m^2\,m^{-2}}$) occur in regions such as the eastern United States (US), southwestern Canada, the western Amazon, and across much of central and Southern Africa (Fig. 1). These responses dominate the MMM zonal mean, yet inter-model agreement is particularly low in the eastern US and central Africa as indicated by low ensemble agreement (i.e., fewer than three out of four models agree on the sign of change) and a large zonal mean spread. In regions with the strongest positive ΔLAI signals, the LUH2 forcing primarily prescribes greater fractions of forest and natural non-forest at the expense of cropland and grazing land, consistent with preservation of natural ecosystems under the sustainable pathway (Fig. S1). Models that provide land-cover output show largely corresponding patterns of natural-vegetation preservation (Fig. S2). However, ΔLAI signals of the individual models diverge from the MMM (Fig. 1b–e).

https://doi.org/10.5194/egusphere-2026-513
Preprint. Discussion started: 23 March 2026

Conversely, the largest and most spatially extensive negative LAI response ($\leq -0.5\ \mathrm{m^2\ m^{-2}}$) occurs over southeastern China (Fig. 1). In this region, the LULCC forcing under the sustainable pathway prescribes lower fractions of forest and natural non-forest and a higher cropland share (Fig. S1). Although this forcing may seem counterintuitive at first, it reflects cropland expansion for second-generation bioenergy under SSP1, particularly in high-productivity regions such as eastern China (Hurtt et al., 2020). The individual model responses accordingly show greater cropland fractions in southeastern China, corresponding to a consistent negative LAI response (Figs. 1 and S2)

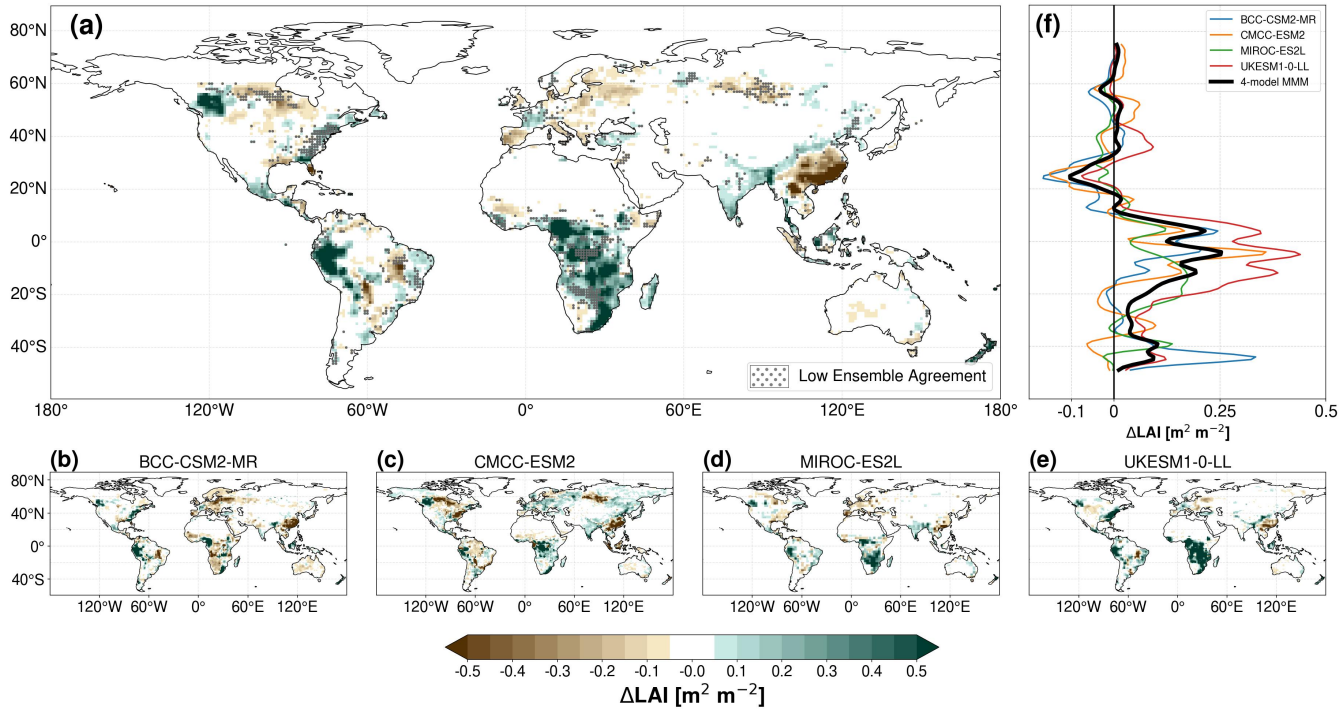

Figure 1. Late-21st-century (2070–2099) difference in LAI associated with sustainable LULCC [$\mathrm{m^2\ m^{-2}}$]. Panels **(a)**–**(e)** show the spatial distribution for the four-model MMM (**a**) and the individual models BCC-CSM2 (**b**), CMCC-ESM2 (**c**), MIROC-ES2L (**d**), and UKESM1 (**e**). Differences within the range $\pm 0.05\ \mathrm{m^2\ m^{-2}}$ are shown in white. In the MMM, regions with low ensemble agreement (fewer than three out of four models agreeing on the sign of ΔLAI) are indicated. Panel **(f)** shows zonal-mean ΔLAI.

Figure 2 maps responses in GPP to sustainable LULCC, which are strongly associated with ΔLAI (MMM spatial Pearson correlation $r = 0.89$ across global land grid cells). Yet, signal magnitudes and signs of ΔGPP and ΔLAI differ in some regions, reflecting their non-linear relationship. For example, modest negative ΔLAI in the western Sahel coincides with pronounced negative ΔGPP in the MMM. Here, the sustainable LUH2 forcing prescribes the ESMs to preserve natural non-forest and pasture at the expense of cropland (Figs. S1 and S2). This disparity between the LAI and GPP response likely reflects that crop PFTs can exhibit higher photosynthetic capacity per unit leaf area than the natural non-forest vegetation and pasture retained under sustainable LULCC. Across individual ESMs, ΔGPP and ΔLAI in the western Sahel diverge further, with mixtures of

https://doi.org/10.5194/egusphere-2026-513
Preprint. Discussion started: 23 March 2026

positive and negative signals (Figs. 1 and 2). The strength of the ΔGPP–ΔLAI relationship also varies by model, with spatial Pearson correlations from $r = 0.66$ (UKESM1) to $r = 0.83$ (BCC-CSM2) across global land grid cells. Lower correlations indicate a more non-linear relationship of GPP and LAI responses and underscore the added value of considering GPP in addition to LAI to capture vegetation responses to LULCC forcing. Although all ESMs are forced by the same LULCC forcing dataset (LUH2), inter-model agreement on vegetation responses is only weak to moderate (pairwise spatial Pearson correlation r ranges: LAI 0.17-0.51; GPP 0.00-0.31). Agreement is weaker for GPP, leading to cancellation in zonal means and a muted MMM signal (Fig. 2f), with an exception around $\sim 10°$N-20°S where zonal-mean ΔGPP is positive across much of the tropics.

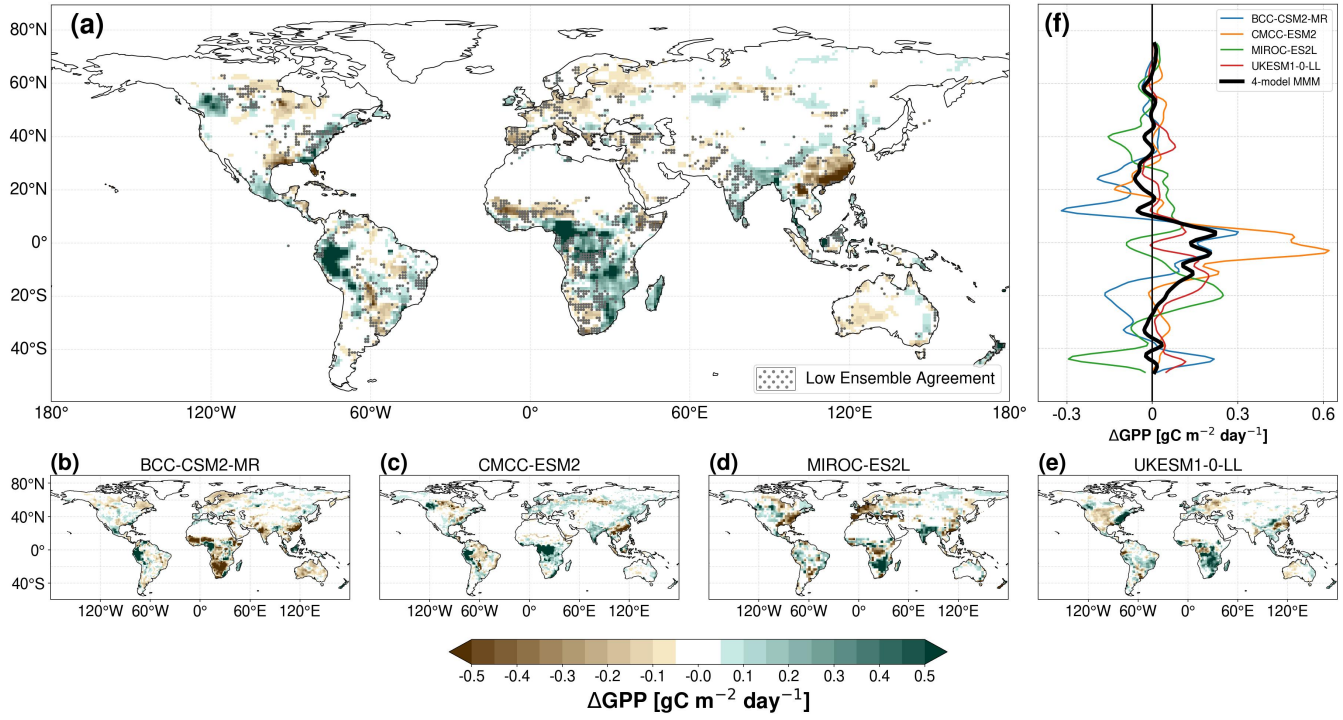

Figure 2. Late-21st-century (2070–2099) difference in GPP associated with sustainable LULCC [$\mathrm{gC\,m^{-2}\,day^{-1}}$]. Panels **(a)–(e)** show the spatial distribution for the four-model MMM (**a**) and the individual models BCC-CSM2 (**b**), CMCC-ESM2 (**c**), MIROC-ES2L (**d**), and UKESM1 (**e**). Differences within the range ± 0.05 $\mathrm{gC\,m^{-2}\,day^{-1}}$ are shown in white. In the MMM, regions with low ensemble agreement (fewer than three out of four models agreeing on the sign of ΔGPP) are indicated. Panel **(f)** shows zonal-mean ΔGPP.

3.2 Impacts of sustainable LULCC on blue–green water partitioning

Sustainable LULCC-induced differences in LAI and GPP impact blue–green water partitioning primarily through their influence on transpiration (Fig. S8). BGWS patterns under SSP1–2.6 and SSP3–7.0 climates remain almost unchanged when land use is swapped (spatial correlations $r \geq 0.98$ across models), while the land-median fractional relative BGWS impact attributable to sustainable LULCC (i.e. I_{BGWS}) is ~5.2 % for the MMM. This indicates that LULCC primarily modulates the magnitude of blue–green water partitioning rather than reorganising its global spatial pattern.

https://doi.org/10.5194/egusphere-2026-513
Preprint. Discussion started: 23 March 2026

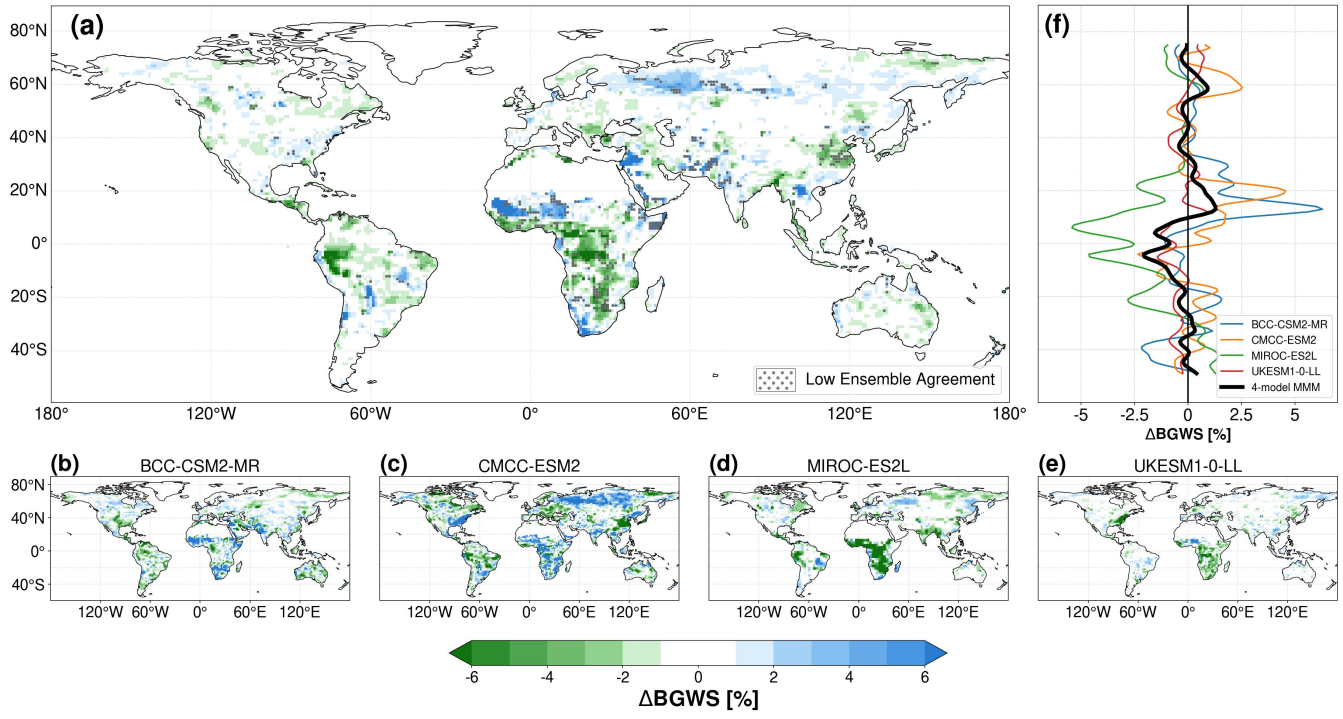

Figure 3. Late-21st-century (2070–2099) difference in BGWS associated with sustainable land use %. Panels **(a)**–**(e)** show the spatial distribution for the four-model MMM (**a**) and the individual models BCC-CSM2 (**b**), CMCC-ESM2 (**c**), MIROC-ES2L (**d**), and UKESM1 (**e**). Positive values indicate a higher blue water share under the sustainable land-use pathway. Differences within the range ±1 % are shown in white. In the MMM, regions with low ensemble agreement (fewer than three out of four models agreeing on the sign of ΔBGWS) are indicated. Panel **(f)** shows zonal-mean ΔBGWS.

Figure 3 shows the spatial distribution of the BGWS response to sustainable LULCC for the MMM (a) and each individual model (b–e), together with the corresponding zonal means (f). Despite only weak inter-model coherence (pairwise spatial Pearson correlations r across the four models range from -0.14 to 0.25), several regionally consistent tendencies emerge in the MMM. Larger green water shares (i.e., negative ΔBGWS) appear across regions such as the western Amazon, the western coast of Africa, and broad parts of Central and Southern Africa (Fig. 3). These regions also generally exhibit substantially positive ΔLAI and ΔGPP, corresponding to increased transpiration (Figs. 1, 2 and S8). Smaller negative ΔBGWS signals occur in Central America, northeastern China and southeastern Europe, notably in regions where ΔGPP and ΔLAI signals are not consistently positive (Figs. 1 and 2). In contrast, greater blue water shares (i.e., positive ΔBGWS) appear, for example, along much of the Sahel into the Horn of Africa, in parts of Southern Africa, in the Levant, and more weakly in western Siberia (Fig. 3). MMM zonal means range around zero, reflecting cancellation of model-specific signals, with MIROC-ES2L notably favouring larger green water shares across most latitudes (Fig. 3f). Nonetheless, three features emerge, namely (i) tendencies toward larger blue water shares in the northern outer tropics (10°–23.5° N), dominated by the Sahel signal; (ii) tendencies toward larger green water shares across the northern inner tropics and the southern tropics (10°N-23.5°S), dominated by re-

https://doi.org/10.5194/egusphere-2026-513
Preprint. Discussion started: 23 March 2026

sponses in the western Amazon, the western coast of Africa, and Central Africa; and (iii) a weaker blue water share dominance near 60°N, dominated by the western Siberia signal.

In the tropics (23.5° S–23.5° N), the MMM zonal-mean BGWS response shows a clear seasonal structure linked to the migration of the ITCZ and associated monsoon systems (Fig. S5). Green water shares are larger during the respective dry seasons north (approximately DJF–MAM) and south (approximately JJA–SON) of the equator, associated with enhanced GPP and transpiration under the sustainable LULCC pathway. Blue water shares are particularly larger during parts of the wet season in the northern tropics (JJA–SON), coinciding with stronger monsoon rainfall and temporarily weaker transpiration. Outside the tropics, zonal-mean BGWS anomalies are generally small, as opposite-signed regional responses partly cancel, and where signals do emerge they are governed mainly by relatively small changes in precipitation and runoff.

The magnitudes and signs of the LAI, GPP and BGWS responses to sustainable LULCC are not always proportional, consistent with non-linear controls and modulation by precipitation (Figs. 1, 2, 3 and S6). For example, strong positive ΔLAI and ΔGPP signals in the eastern US and southwestern Canada do not translate into proportionally larger green water shares. By contrast, other regions with similarly strong increases in ΔLAI and ΔGPP, such as the western Amazon, show a strong positive ΔBGWS signal (Fig. 3). Comparing the precipitation signal in these three regions shows a positive precipitation response in the eastern US and southwestern Canada, whereas the western Amazon primarily exhibits drying conditions (Fig. S6).

In the eastern US, forest preservation relative to cropland is associated with larger gains in runoff (area-weighted mean: $+0.06\ \mathrm{mm\,day^{-1}}$) than in transpiration (area-weighted mean: $+0.04\ \mathrm{mm\,day^{-1}}$) (Figs. S7 and S8). This suggests that, in terms of blue–green water partitioning, the additional precipitation exceeds the higher transpiration demand associated with higher LAI and GPP. As a result, the net effect corresponds to larger blue water shares, although inter-model uncertainty in the ecohydrological responses remains substantial (see Subsection 3.3). In southwestern Canada, runoff responses in forest-preserved grid cells are weak (area-weighted mean: $0.00\ \mathrm{mm\,day^{-1}}$) and spatially heterogeneous despite robust precipitation increases (area-weighted mean: $+0.07\ \mathrm{mm\,day^{-1}}$). Accordingly, precipitation differences show only a weak association with runoff differences ($r = 0.03$), implying that additional precipitation is not efficiently converted into blue water. Instead, precipitation anomalies are more strongly associated with increased evaporation (including interception) ($r = 0.93$) and increased surface soil moisture ($r = 0.6$) (Figs. S9 and S10). As a result, BGWS changes remain comparatively small in southwestern Canada even under strong forest preservation, because the precipitation increase is partitioned into other land-surface fluxes and storage rather than primarily into runoff (or transpiration). This precipitation-driven damping contrasts with the western Amazon, where drying conditions amplify BGWS changes through a shrinking precipitation denominator.

The precipitation changes associated with sustainable LULCC can reflect both changes in large-scale circulation (i.e. a re-distribution of atmospheric moisture) and enhanced local land–atmosphere coupling through moisture recycling. In the three example regions, the correlation between LULCC-induced anomalies in ET and precipitation is much stronger in the eastern US ($r = 0.81$) and southwestern Canada ($r = 0.94$) than in the western Amazon ($r = 0.21$), suggesting a tighter local ET–precipitation co-variability (Figs. S6 and S11). However, these correlations alone do not distinguish whether ET drives precipitation via local recycling, or whether both, precipitation and ET, respond to circulation-driven changes in atmospheric moisture supply. Important to note here is the timing of the additional precipitation in the extratropical example regions. In

https://doi.org/10.5194/egusphere-2026-513
Preprint. Discussion started: 23 March 2026

the eastern US the additional precipitation falls in Northern Hemisphere spring (MAM) and summer (JJA) (Fig. S15), while in southwestern Canada in winter (DJF) and spring (MAM) (not shown).

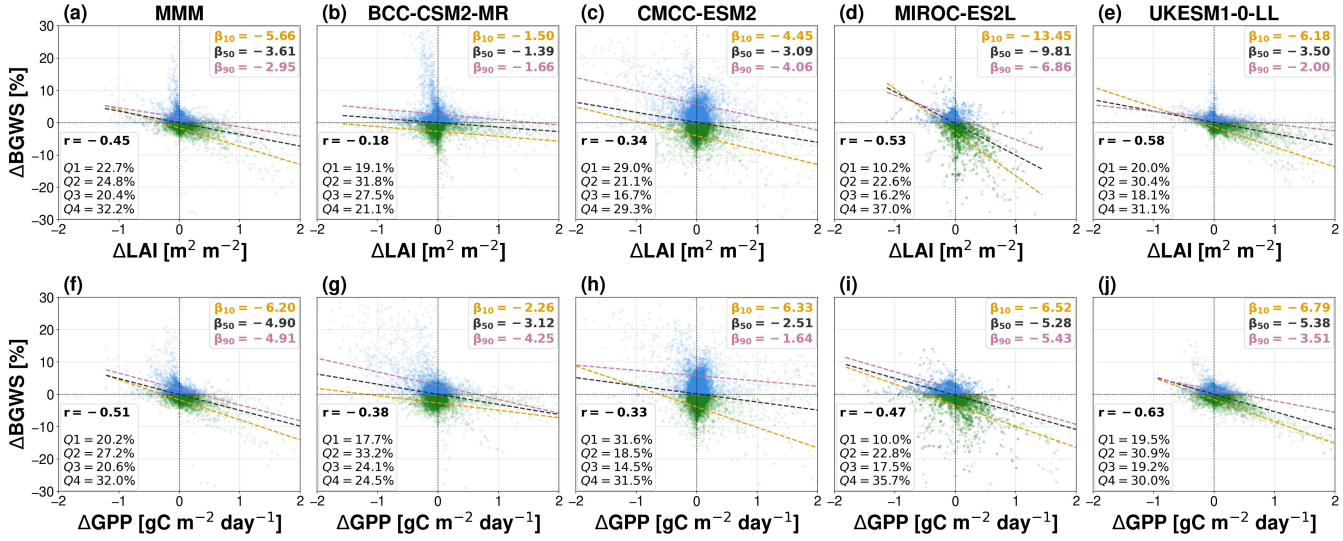

Figure 4. Quantile regression between late-21st-century (2070–2099) differences in BGWS [%] and differences in LAI [$m^2\ m^{-2}$] and GPP [$gC\ m^{-2}\ day^{-1}$] associated with sustainable LULCC. Panels **(a)**–**(e)** show quantile regressions between ΔBGWS and ΔLAI for the four-model MMM (**a**) and the individual models BCC-CSM2-MR (**b**), CMCC-ESM2 (**c**), MIROC-ES2L (**d**), and UKESM1-0-LL (**e**). Panels **(f)**–**(j)** show the corresponding relationships between ΔBGWS and ΔGPP. Quantile regressions are shown for the 10th, 50th, and 90th percentiles. The slope coefficient β_1 denotes the change in ΔBGWS per unit LAI or GPP difference at each quantile. Pearson's correlation coefficient (r) is reported for the full sample. The fraction of grid cells in each quadrant is indicated: Q1, positive ΔBGWS and LAI/GPP difference; Q2, positive ΔBGWS and negative LAI/GPP difference; Q3, negative ΔBGWS and LAI/GPP difference; and Q4, negative ΔBGWS and positive LAI/GPP difference.

Similarly, negative LAI and GPP responses do not always correspond to larger blue water shares. One such example is the blue–green water partitioning response to the LAI and GPP decrease in eastern China. In southeastern China, cropland expansion is associated with a weak increase in blue water share, partially muted by a negative precipitation response (Figs. 3, S1, S2 and S6). Northeastern China, in contrast, shows a strong increase in green water shares (negative ΔBGWS; Fig. 3). Here, LUH2 forcing prescribes preservation of natural non-forest and reduced grazing land fractions (Fig. S1), and the ESMs translate this forcing into increased primary and secondary vegetation cover, while pasture fractions decline (Fig. S2). Over much of northeastern China, the preservation of primary and secondary vegetation over pasture is associated with negative ΔLAI and ΔGPP and negligible transpiration changes. As a consequence, the larger green water shares in the southern part of northeastern China arise mainly from reduced precipitation and corresponding runoff declines, along with lower surface soil moisture (Figs. S6, S7 and S9). Precipitation responses to sustainable LULCC can even induce substantial blue–green water partitioning changes in regions with weak LAI and GPP responses, such as western Siberia (40°–70° E, 50°–70° N). There, larger blue water shares are linked to higher precipitation and runoff, while land-use changes are negligible and transpiration

https://doi.org/10.5194/egusphere-2026-513
Preprint. Discussion started: 23 March 2026

remains nearly unchanged (Figs. 3, S2, S6, S7, and S8). This indicates that non-local effects of LULCC elsewhere modify atmospheric moisture transport and the associated precipitation regimes.

The non-linear relationship between vegetation responses and BGWS changes is reflected in moderate negative spatial correlations between ΔBGWS and ΔLAI ($r = -0.45$) and between ΔBGWS and ΔGPP ($r = -0.51$; Fig. 4), indicating that regions with stronger vegetation increases generally shift toward larger green water shares. While the MMM indicates a slightly stronger coupling of ΔBGWS to ΔGPP than to ΔLAI, this association holds only true for BCC-CSM2 and MIROC-ES2L and is therefore not robust across models (Fig. 4). Quantile regressions of the conditional ΔBGWS distributions show steeper slope magnitudes (β_1) at the 10$^{\text{th}}$ percentile ($\tau = 0.10$) than at the 90$^{\text{th}}$ percentile ($\tau = 0.90$) for both predictors ($X \in \{\Delta\text{LAI}, \Delta\text{GPP}\}$). Because negative ΔBGWS denotes a shift toward larger green water shares, this implies that grid cells exhibiting the strongest green water gains (lower tail) are more sensitive per unit change in ΔLAI or ΔGPP than cells in the upper tail (tail asymmetry). One notable exception is BCC-CSM2, where ΔBGWS–ΔLAI correlations are weak, indicating a partial decoupling between leaf area changes and blue–green water partitioning at the global grid-cell scale. Interestingly, the MMM tail asymmetry reverses in the historical (deforestation-dominated) experiments, where $|\beta_1(0.90)| > |\beta_1(0.10)|$, consistent with stronger sensitivity of blue water increases to vegetation losses (Fig. S3).

3.3 Regional differences in model-specific vegetation and blue–green water partitioning responses

To illustrate differences in model-specific vegetation and blue–green water partitioning responses, we highlight the eastern United States (30°–45° N, 90°–70° W). In this region, the LUH2 forcing prescribes higher forest fractions due to afforestation and avoided deforestation in SSP1, in contrast to cropland expansion and forest loss in SSP3 (Fig. S1).

A first source of inter-model uncertainty arises from the translation of the LUH2 forcing into model-specific land-cover data (Loughran et al., 2023). For the models providing the required output (excluding BCC-CSM2), there is a modest to strong correspondence between the prescribed LUH2 forest and cropland differences and the simulated land-cover responses in the eastern US (Figs. S1, S2, and Table S2). For forest cover, spatial correlations between LUH2 and the model-specific responses range from $r = 0.59$ in MIROC-ES2L to $r = 0.83$ in CMCC-ESM2 and UKESM1-0-LL. Sign agreement exceeds 79 % for all forest differences. Cropland differences also show good agreement, with correlation coefficients between 0.60 and 0.83 and sign agreement close to or above 75 % across models. These metrics indicate that the direction of land-use change in the eastern US is consistently captured by the models, while the magnitude of the differences shows a wider inter-model spread. Still, the simulated ecohydrological responses to sustainable LULCC in the eastern US show substantial inter-model differences in both sign and magnitude (Fig. 5).

https://doi.org/10.5194/egusphere-2026-513
Preprint. Discussion started: 23 March 2026

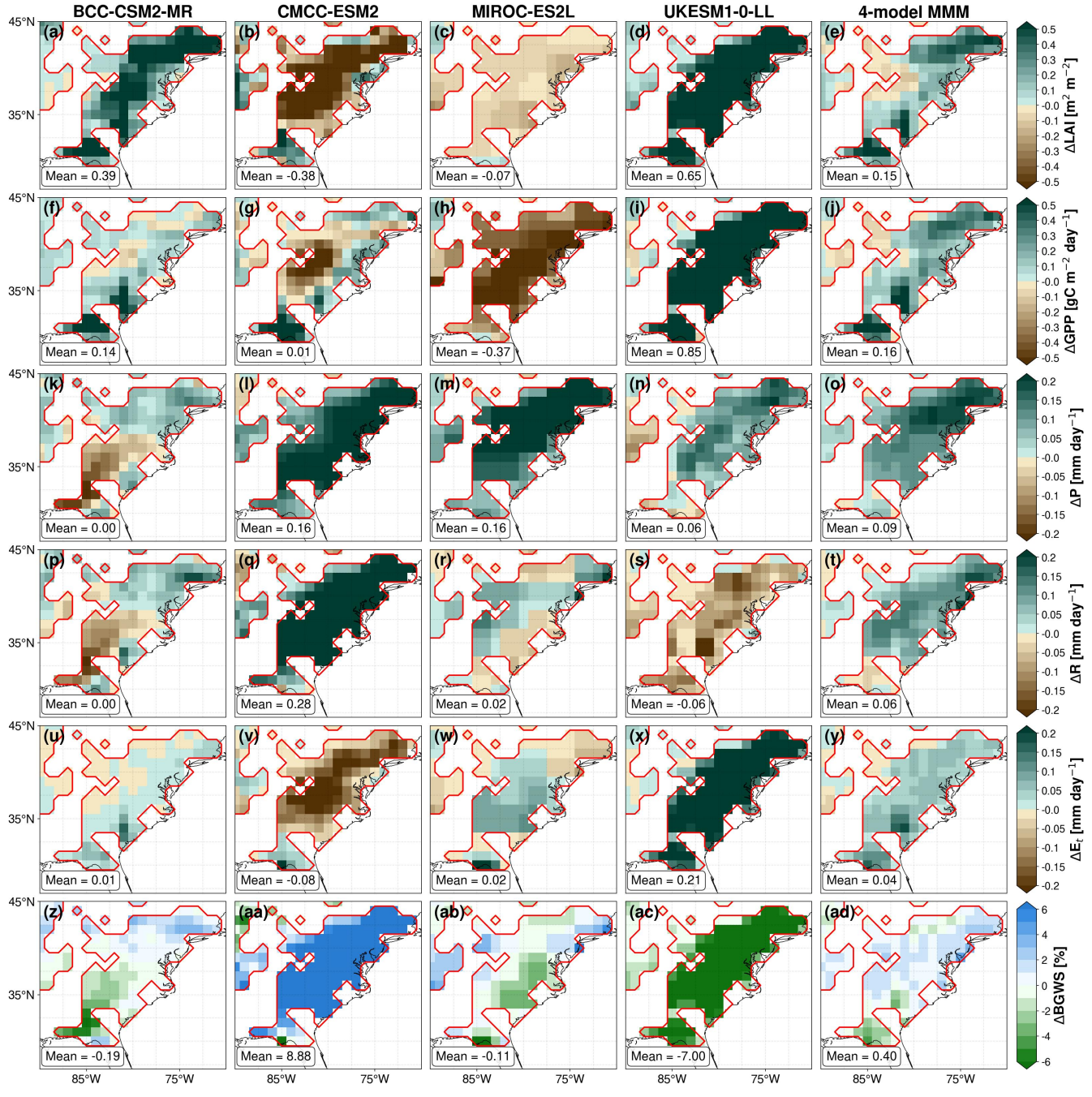

Figure 5. Late-21st-century (2070–2099) differences in ecohydrological variables associated with sustainable LULCC over the eastern United States (30°–45° N, 90°–70° W). Panels show results for the four-model MMM and the individual models. Only grid cells where LUH2 prescribes higher forest fractions and lower cropland fractions under the sustainable pathway are shown. The boundary of this forest-for-cropland mask is indicated in red. For each variable and model, the arithmetic mean over the masked grid cells is reported. Variables shown are ΔLAI, ΔGPP, ΔP, ΔR, ΔE_t, and ΔBGWS.

https://doi.org/10.5194/egusphere-2026-513
Preprint. Discussion started: 23 March 2026

Both BCC-CSM2 and UKESM1 simulate positive GPP and LAI responses to the higher forest fractions. However, the response in BCC-CSM2 is weaker, and ΔGPP is clearly positive only over the southeastern US. In this model, ΔGPP is negative in Northern Hemisphere spring (MAM) but positive for the rest of the year, suggesting that crops are parametrised to have higher springtime productivity than forests (Fig. S13). By contrast, UKESM1 shows positive seasonal GPP responses to afforestation throughout the year. Consequently, transpiration increases across most of the eastern US in UKESM1, whereas BCC-CSM2 shows only weak increases confined to the southeastern US. BCC-CSM2's transpiration response thus corresponds strongly to the GPP pattern, with a Pearson correlation of $r = 0.95$ across all eastern US forest-for-cropland grid cells. The relationship to LAI is much weaker (Pearson correlation $r = 0.66$), indicating that changes in plant productivity exert a stronger control on transpiration than changes in leaf area in this model.

In UKESM1, the positive transpiration response is accompanied by higher total evapotranspiration and increased precipitation over the eastern US (Fig. S20). This additional precipitation is not partitioned into higher runoff. Instead, runoff tends to decrease slightly, while transpiration and surface soil moisture increase (Fig. S18). As a result, ΔBGWS is negative, indicating a shift towards larger green water shares. This response may be influenced by UKESM1's interactive vegetation scheme (TRIFFID), which allows prognostic vegetation states and PFT competition within prescribed land-use units, potentially reinforcing transpiration under wetter conditions. In BCC-CSM2, changes in evapotranspiration are weaker and more heterogeneous (Fig. S20). In the southeastern US, where GPP and transpiration increase, precipitation tends to decrease, and an even smaller fraction of this reduced input is routed to runoff, reinforcing green water shares. In the northeastern US, precipitation increases and a larger fraction is partitioned into runoff, leading to locally larger blue water shares while transpiration changes remain modest. In contrast, UKESM1 shows consistently larger green water shares across the eastern US, reflecting a strong coupling between higher forest fractions over cropland and larger green water shares (Pearson correlation $r = -0.79$ across eastern US forest-for-cropland grid cells).

The direction of the blue–green water partitioning response to higher forestation over cropland in the eastern US is further complicated by CMCC-ESM2 and MIROC-ES2L. In CMCC-ESM2, ΔLAI is positive in the southeastern US and negative in the northeastern US. The GPP response is similar, although positive ΔGPP also extends along parts of the northeastern coast. CMCC-ESM2 shows a strong seasonality in the LAI and GPP responses, with positive signals in Northern Hemisphere summer (JJA) but predominantly negative responses in the colder months (Figs. S12 and S13). The southeastern US is an exception, where LAI and GPP responses to larger forest fractions are positive year-round. This pattern suggests that, in colder climates, the forest PFTs in CMCC-ESM2 are represented as having smaller and less productive leaves and a strong phenological cycle compared to the crop PFTs, whereas under warmer conditions forests become more productive than crops throughout the year.

In comparison, MIROC-ES2L explicitly shows negative LAI and, in particular, GPP responses to forest expansion in the eastern US year-round. This response is consistent with strong nutrient constraints (high vegetation C:N ratios), which are more pronounced than in UKESM1 (the only other model providing vegetation nitrogen; Fig. S21). Under these conditions, forest carbon in MIROC-ES2L accumulates primarily in woody biomass, while reduced leaf carbon and the lower specific leaf area (SLA) of forest relative to crop leaves jointly suppress LAI and thereby GPP. In contrast, UKESM1 exhibits a strong increase in leaf carbon that outweighs its SLA reduction, consistent with the higher LAI and GPP simulated under forest expansion.

https://doi.org/10.5194/egusphere-2026-513
Preprint. Discussion started: 23 March 2026

The negative GPP and LAI responses simulated by CMCC-ESM2 and MIROC-ES2L for forestation over cropland in the eastern US stand in contrast to the positive vegetation responses in BCC-CSM2 and UKESM1. These differences also affect how vegetation changes translate into transpiration, leaving substantial uncertainty about the ecohydrological consequences of sustainable LULCC in the region. Although the vegetation response in CMCC-ESM2 contrasts with that of BCC-CSM2 and UKESM1, the coupling between LAI and transpiration in eastern US forest-for-cropland grid cells is comparable, with a Pearson correlation of $r = 0.87$. This suggests that, if CMCC-ESM2 also simulated larger GPP and LAI under forestation over cropland, similar shifts in blue–green water partitioning could be expected. Instead, CMCC-ESM2 shows increased precipitation and runoff, while transpiration declines, leading to a shift towards larger blue water shares. Compared to BCC-CSM2, transpiration in CMCC-ESM2 is more strongly tied to LAI in eastern US forest-for-cropland grid cells.

Unlike the other models, MIROC-ES2L displays an almost complete decoupling of transpiration from vegetation responses for forestation over cropland in the eastern US, with Pearson correlations close to zero. This decoupling is not consistent with the global relationship in MIROC-ES2L for forest-for-cropland grid cells, where transpiration correlates moderately with LAI ($r = 0.59$) and GPP ($r = 0.49$), and it highlights the importance of regional environmental conditions for vegetation–transpiration coupling. A possible reason for the slight increase in transpiration despite lower LAI and GPP is the higher soil moisture availability in preserved forest areas (Fig. S18), which can sustain transpiration locally and partly decouple green water fluxes from the GPP and LAI responses. In addition, greater aerodynamic roughness, canopy conductance, and deeper rooting profiles of forest PFTs compared to crop PFTs as well as forest–cropland albedo contrasts and associated surface-energy balance changes may further contribute to this decoupling. Although transpiration increases only weakly, MIROC-ES2L simulates a strong increase in ET, dominated by enhanced evaporation (Figs. S19 and S20). Precipitation also increases markedly, which likely reflects both enhanced local moisture recycling and additional moisture influx from non-local sources. This precipitation response is accompanied by higher runoff, so that the blue–green water partitioning in MIROC-ES2L remains relatively constant.

4 Discussion and conclusions

In this study, we use LUMIP simulations from four ESMs to analyse global blue–green water partitioning changes under sustainable LULCC (i.e., predominantly avoided deforestation and preservation of natural non-forest ecosystems) using the BGWS metric. We find that LULCC substantially impacts BGWS through transpiration changes and precipitation feedbacks. At the global scale, LULCC primarily modulates the magnitude of BGWS rather than reorganising its large-scale spatial pattern, suggesting that the dominant controls on the global distribution of blue versus green water remain set by the background climate state. Whether sustainable LULCC corresponds to larger blue or green water shares depends on the land-cover conversion type (e.g., forest versus cropland), regional hydroclimatic conditions and land–atmosphere coupling strength (e.g., ET–precipitation co-variability), and the influence of non-local moisture transport. The blue–green water partitioning responses of ESMs show pronounced inter-model uncertainty in many regions, as illustrated by the eastern US case study (Sect. 3.3).

https://doi.org/10.5194/egusphere-2026-513
Preprint. Discussion started: 23 March 2026

Larger forest fractions, mostly related to higher LAI and GPP, generally correspond to larger green water shares. This aligns with regional climate modelling evidence that forestation can shift water partitioning from blue to green fluxes, that is, "forestation turns blue water green" (Asselin et al., 2024). The quantile regression analysis further shows a higher sensitivity of the lower (green) ΔBGWS tail (10^{th} percentile) to one-unit change in ΔLAI and ΔGPP than the median response and the upper (blue) ΔBGWS tail (90^{th} percentile). This indicates an asymmetric response, where greening associated with afforestation and avoided deforestation can induce comparatively strong per-unit shifts in blue–green partitioning. Conversely, analysis of the historical experiments with intensive LULCC suggests that vegetation declines are associated with a stronger sensitivity in the upper (blue) tail of the ΔBGWS distribution. Taken together, these results imply that the direction of vegetation change (loss versus gain) modulates not only the sign but also the magnitude of partitioning shifts. This nonlinearity cautions that both deforestation and large-scale restoration can produce disproportionate impacts on regional blue–green water availability.

The relationship of higher LAI and GPP amplifying green water shares is non-linear and depends on the precipitation response to LULCC, which is the primary control on blue water flow generation. The fact that responses in ET and precipitation are tightly correlated in the eastern US and southwestern Canada, but only weakly correlated in the western Amazon, points to regional differences in the balance between local moisture recycling and large-scale atmospheric moisture transport changes. This interpretation aligns with evidence that vegetation can affect water availability not only locally (through ET and local precipitation) but also non-locally through atmospheric moisture recycling and downwind moisture supply from upwind ET, meaning that precipitation responses may depend on upwind land-surface change as much as on local ET (Cui et al., 2022; Hoek van Dijke et al., 2022; Tuinenburg et al., 2020). In the eastern US, the strong ET–precipitation co-variability, particularly in the summer months (JJA), is consistent with observational diagnostics indicating that higher ET enhances the probability of summer afternoon rainfall in the region (Findell et al., 2011). The larger blue water shares in the eastern US emphasise that vegetation–precipitation feedbacks can mediate the simple "more LAI causes less blue water" paradigm. Here, the additional green water demand is offset by additional precipitation input, reducing the adverse impacts of these measures for local blue water availability. The additional winter and spring precipitation in southwestern Canada is unlikely to be caused by stronger local moisture recycling since land precipitation recycling is lowest in winter and peaks in summer (Tuinenburg et al., 2020). Thus, this regional wetting tends to be associated with increased moisture from the ocean rather than increased land recycling (Staal et al., 2025). Our results show that the precipitation gain in southwestern Canada is partitioned mostly into evaporation and storage rather than into additional blue water generation. This is supported by findings of Cui et al. (2022) who identify western Canada as a region where vegetation growth can reduce water availability ($P - ET$) regionally and downwind.

Studies on land-use and precipitation feedbacks in the Amazon basin show that a substantial fraction of rainfall is sustained by moisture recycled within the basin itself (e.g., Spracklen et al., 2012; Staal et al., 2018; Tuinenburg et al., 2020; Wang-Erlandsson et al., 2018). In particular, forests in the southern and central Amazon act as major moisture sources, while forests in the south-western Amazon depend strongly on transpired-water subsidies from upwind parts of the basin (Staal et al., 2018). In our sustainable land-use pathway (L1), forest fractions in the western Amazon increase strongly (avoided deforestation of up to ∼40 %), whereas forest cover changes in many upwind parts of the basin remain comparatively small (typically <5 %). This spatial pattern is consistent with the limited precipitation response we find over the western Amazon. Here, strong local

https://doi.org/10.5194/egusphere-2026-513
Preprint. Discussion started: 23 March 2026

forest preservation alone does not appear sufficient to trigger large additional rainfall if forest cover in key moisture source regions changes only weakly. This underpins the idea that afforestation and avoided deforestation measures in regions with weaker local LULCC–precipitation coupling alone, such as the western Amazon, may result in a blue water scarce environment. Hence, these measures should include information about forest-rainfall cascades to balance impacts on blue and green water availability (Staal et al., 2018). Placing our LUMIP-isolated precipitation response in the context of ScenarioMIP SSP differences, recent studies indicate that Amazon hydroclimate and terrestrial moisture recycling across SSPs are often dominated by the background warming and CO_2 physiological signal rather than land-cover change alone (Engel et al., 2025; Li et al., 2023; Staal et al., 2025). Accordingly, the lower precipitation in SSP3-7.0 compared to SSP1-2.6 over the western Amazon can largely reflect the climate component, while the isolated L1–L3 land-use precipitation response can remain weak and may even differ in sign locally, depending on how forest changes project onto key upwind moisture-source regions and associated moisture-transport pathways. Moisture-tracking studies provide a useful first-order estimate of recycling impacts, but they are diagnostic frameworks that do not simulate the circulation response to altered tree cover and therefore cannot capture forest-induced circulation adjustments (Engel et al., 2025; Hoek van Dijke et al., 2022; Tuinenburg et al., 2020; Spracklen et al., 2012; Staal et al., 2018). By contrast, the fully coupled ESM experiments analysed here explicitly resolve circulation adjustments and associated local and non-local precipitation responses to forest cover change (Fahrenbach et al., 2025; Portmann et al., 2022; De Hertog et al., 2023).

As shown in Subsection 3.3, our findings are highly model dependent. The dilemma of uncertain but significant LULCC impacts across ESMs has long been recognised (e.g., Boysen et al., 2020; Pitman et al., 2009; Santos et al., 2023) and, despite the harmonised LUH2 forcing and protocol of LUMIP (Lawrence et al., 2016), remains substantial in the CMIP6 land-use experiments analysed here. This is well illustrated by the eastern US, where the same LUH2 land-use forcing yields contrasting blue–green water partitioning responses across models, ranging from consistently larger blue water shares in CMCC-ESM2, to weak and mixed responses in BCC-CSM2-MR and MIROC-ES2L, to consistently larger green water shares in UKESM1. In UKESM1 and CMCC-ESM2, the contrasting partitioning outcomes appear to arise primarily from differences in the simulated vegetation response to the same afforestation and avoided deforestation forcing. In MIROC-ES2L and BCC-CSM2-MR, by contrast, the coupling between vegetation change and the ecohydrological response is weaker and less linear, indicating a stronger role for model-specific process representations in translating ΔLAI/ΔGPP into changes in blue–green water partitioning. Together, these contrasts highlight the need for a multi-model approach to constrain process understanding and to assess region-specific consequences of LULCC, rather than relying on a single-model estimate.

Consistent with earlier assessments, we interpret this spread as arising from four main sources. First, inter-model uncertainty arises when the LUH2 transitions are translated into each model's internal land-cover map (Loughran et al., 2023). In the eastern US example, however, the direction of the imposed land-use change is represented consistently by the model ensemble, while the magnitude of the realised land-cover anomalies shows a larger inter-model spread. Second, models differ in how fractional land-cover changes are mapped to PFTs and in whether vegetation cover fractions can adjust interactively via competition (Di Vittorio et al., 2014). For example, definitions of forest and tree cover differ among models, depending on how LUH2 classes are mapped to PFTs (Loughran et al., 2023). In our ensemble, interactive PFT competition is represented

https://doi.org/10.5194/egusphere-2026-513
Preprint. Discussion started: 23 March 2026

explicitly only in UKESM1, where PFT fractions can adjust to climate and land-surface changes within the prescribed natural and managed land units via the TRIFFID vegetation scheme (Sellar et al., 2019; Burton et al., 2019). This may strengthen local ecohydrological feedbacks; for example, in the eastern US, increased precipitation in UKESM1 coincides with higher transpiration and reduced runoff, consistent with a vegetation–atmosphere coupling that can be reinforced when vegetation states respond prognostically to hydroclimatic changes. However, explicit information on grid-cell specific PFT compositions is not available as standard CMIP6 output for these experiments. Making such output available in future ESM simulations would allow a more in-depth attribution of inter-model uncertainty to PFT mapping and within-grid composition in multi-model assessments. Third, land-surface biogeochemistry and plant trait parametrisations (e.g., photosynthetic capacity, phenology) vary substantially across ESMs (Pitman et al., 2009; Boysen et al., 2020). Moreover, models differ in their treatment of nutrient limitation, with some including explicit terrestrial C–N coupling (e.g., MIROC-ES2L), whereas BCC-CSM2 is the only model in our ensemble documented without an interactive terrestrial nitrogen cycle (Table 1) (Arora et al., 2020). Taken together, these model differences mean that similar land-cover anomalies can produce markedly different changes in vegetation function, including LAI and GPP. This underscores that robust assessments of LULCC impacts require considering not only land-cover fractions, but also how models represent vegetation physiology and biogeochemical constraints. Fourth, differences in land energy–water coupling and hydrological parametrisations (e.g., evapotranspiration partitioning, soil-moisture stress, and runoff generation) can amplify small vegetation differences into divergent runoff and transpiration responses (Berg and Sheffield, 2019; Fu et al., 2024; Decharme, 2007).

In addition to the inter-model spread discussed above, our analysis has several limitations. The BGWS metric relies on runoff and transpiration and therefore does not explicitly account for other pathways and storages that can modulate water availability, including interception and soil evaporation, changes in soil-moisture and groundwater storage, and lateral redistribution within the land surface. This matters in regions where precipitation anomalies are primarily buffered by evaporation and storage rather than converted into runoff, as illustrated by southwestern Canada in our results. None of the four CMIP6 ESMs used here apply explicit irrigation in their CMIP6 simulations (Al-Yaari et al., 2022), which likely overestimates the dry-season contrast between cropland and forest green water shares in the tropics. Irrigation would increase water supply for crops during dry periods, allowing higher productivity and transpiration and thereby increasing cropland green water shares relative to rainfed conditions. Internal variability may still affect the inferred LULCC signal because the number of available ensemble members is limited and uneven across models. However, we mitigate its influence by defining Δ_{LULCC} as a symmetric average across background climates to improve the signal-to-noise ratio and by benchmarking the historical four-model MMM against an extended nine-model MMM, which shows highly consistent spatial patterns. The coarse native resolution of CMIP6 ESMs also constrains interpretation at local scales, and caution is warranted when translating these large-scale, scenario-level responses to smaller reforestation or forest conservation projects where the signal-to-noise ratio may be lower. Finally, while our LUMIP-derived estimate isolates the land-use contribution by construction, it does not remove uncertainty related to the realism of land-use patterns and their spatial alignment with key hydroclimatic gradients and moisture-source regions.

Despite these uncertainties, our results have implications for land-based mitigation and adaptation planning. Sustainable LULCC can alter regional blue–green water partitioning through changes in vegetation water use and precipitation, so evalu-

https://doi.org/10.5194/egusphere-2026-513
Preprint. Discussion started: 23 March 2026

ations of afforestation and avoided deforestation should consider carbon outcomes alongside water-partitioning consequences and their seasonality. In regions such as the Amazon, where precipitation is strongly influenced by upwind moisture supply, the effectiveness and hydrological side effects of local interventions are likely to depend on changes in key moisture-source areas, highlighting the importance of accounting for forest–rainfall cascades. Given the pronounced inter-model spread, robust decision-making benefits from multi-model ensembles and scenario ranges, complemented by monitoring and local water-management options where appropriate.

Code and data availability. The CMIP6/LUMIP datasets used in this study were accessed through the Deutsche Klimarechenzentrum (DKRZ) CMIP Data Pool (last access: 20 June 2025) and the Earth System Grid Federation (https://aims2.llnl.gov) portal. The DKRZ CMIP Data Pool (available at https://cmip-data-pool.dkrz.de) is restricted to registered users with a valid DKRZ account. The LUH2 data was downloaded from the LUH2 website (https://luh.umd.edu/data.shtml). All code to reproduce this analysis is publicly available on Zenodo (DOI: 10.5281/zenodo.18378688) and maintained on GitHub at https://github.com/simonheselschwerdt/LUMIP_bgws.

Author contributions. S.P.H. and P.G. conceived the study and designed the analysis. N.L.S.F. provided methodological input on the separation of the land-use signal. S.P.H. conducted the analysis and led the writing of the manuscript. All authors discussed the methods and results and contributed to writing and edited the manuscript.

Competing interests. The authors declare no competing interests.

Acknowledgements. This study is financially supported by the Helmholtz Association Initiative and Networking Fund (IVF). We acknowledge the World Climate Research Programme's Working Group on Coupled Modelling, which is responsible for CMIP, and we thank the climate modelling groups for producing and making available their model output. This work used resources of the Deutsches Klimarechenzentrum (DKRZ, https://www.dkrz.de) granted by its Scientific Steering Committee (WLA) under project ID ch0636. S.P.H. and P.G. also thank Irem Isik for internally reviewing our paper draft.

https://doi.org/10.5194/egusphere-2026-513
Preprint. Discussion started: 23 March 2026

References

Al-Yaari, A., Ducharne, A., Thiery, W., Cheruy, F., and Lawrence, D.: The Role of Irrigation Expansion on Historical Climate Change: Insights From CMIP6, Earth's Future, 10, e2022EF002 859, https://doi.org/10.1029/2022EF002859, 2022.

Amali, A. A., Schwingshackl, C., Ito, A., Barbu, A., Delire, C., Peano, D., Lawrence, D. M., Wårlind, D., Robertson, E., Davin, E. L., Shevliakova, E., Harman, I. N., Vuichard, N., Miller, P. A., Lawrence, P. J., Ziehn, T., Hajima, T., Brovkin, V., Zhang, Y., Arora, V. K., and Pongratz, J.: Biogeochemical versus biogeophysical temperature effects of historical land-use change in CMIP6, Earth System Dynamics, 16, 803–840, https://doi.org/10.5194/esd-16-803-2025, 2025.

Arora, V. K., Katavouta, A., Williams, R. G., Jones, C. D., Brovkin, V., Friedlingstein, P., Schwinger, J., Bopp, L., Boucher, O., Cadule, P., Chamberlain, M. A., Christian, J. R., Delire, C., Fisher, R. A., Hajima, T., Ilyina, T., Joetzjer, E., Kawamiya, M., Koven, C. D., Krasting, J. P., Law, R. M., Lawrence, D. M., Lenton, A., Lindsay, K., Pongratz, J., Raddatz, T., Séférian, R., Tachiiri, K., Tjiputra, J. F., Wiltshire, A., Wu, T., and Ziehn, T.: Carbon–concentration and carbon–climate feedbacks in CMIP6 models and their comparison to CMIP5 models, Biogeosciences, 17, 4173–4222, https://doi.org/10.5194/bg-17-4173-2020, 2020.

Asselin, O., Leduc, M., Paquin, D., de Noblet-Ducoudré, N., Rechid, D., and Ludwig, R.: Blue in green: forestation turns blue water green, mitigating heat at the expense of water availability, Environmental Research Letters, 19, 114 003, https://doi.org/10.1088/1748-9326/ad796c, 2024.

Berg, A. and Sheffield, J.: Evapotranspiration Partitioning in CMIP5 Models: Uncertainties and Future Projections, Journal of Climate, 32, 2653–2671, https://doi.org/10.1175/JCLI-D-18-0583.1, 2019.

Best, M. J., Pryor, M., Clark, D. B., Rooney, G. G., Essery, R. L. H., Ménard, C. B., Edwards, J. M., Hendry, M. A., Porson, A., Gedney, N., Mercado, L. M., Sitch, S., Blyth, E., Boucher, O., Cox, P. M., Grimmond, C. S. B., and Harding, R. J.: The Joint UK Land Environment Simulator (JULES), model description – Part 1: Energy and water fluxes, Geoscientific Model Development, 4, 677–699, https://doi.org/10.5194/gmd-4-677-2011, 2011.

Bonan, G. B.: Forests and Climate Change: Forcings, Feedbacks, and the Climate Benefits of Forests, Science, 320, 1444–1449, https://doi.org/10.1126/science.1155121, 2008.

Boucher, O., Servonnat, J., Albright, A. L., Aumont, O., Balkanski, Y., Bastrikov, V., Bekki, S., Bonnet, R., Bony, S., Bopp, L., Braconnot, P., Brockmann, P., Cadule, P., Caubel, A., Cheruy, F., Codron, F., Cozic, A., Cugnet, D., D'Andrea, F., Davini, P., de Lavergne, C., Denvil, S., Deshayes, J., Devilliers, M., Ducharne, A., Dufresne, J.-L., Dupont, E., Éthé, C., Fairhead, L., Falletti, L., Flavoni, S., Foujols, M.-A., Gardoll, S., Gastineau, G., Ghattas, J., Grandpeix, J.-Y., Guenet, B., Guez, Lionel, E., Guilyardi, E., Guimberteau, M., Hauglustaine, D., Hourdin, F., Idelkadi, A., Joussaume, S., Kageyama, M., Khodri, M., Krinner, G., Lebas, N., Levavasseur, G., Lévy, C., Li, L., Lott, F., Lurton, T., Luyssaert, S., Madec, G., Madeleine, J.-B., Maignan, F., Marchand, M., Marti, O., Mellul, L., Meurdesoif, Y., Mignot, J., Musat, I., Ottlé, C., Peylin, P., Planton, Y., Polcher, J., Rio, C., Rochetin, N., Rousset, C., Sepulchre, P., Sima, A., Swingedouw, D., Thiéblemont, R., Traore, A. K., Vancoppenolle, M., Vial, J., Vialard, J., Viovy, N., and Vuichard, N.: Presentation and Evaluation of the IPSL-CM6A-LR Climate Model, Journal of Advances in Modeling Earth Systems, 12, e2019MS002 010, 2020.

Boysen, L. R., Brovkin, V., Pongratz, J., Lawrence, D. M., Lawrence, P., Vuichard, N., Peylin, P., Liddicoat, S., Hajima, T., Zhang, Y., Rocher, M., Delire, C., Séférian, R., Arora, V. K., Nieradzik, L., Anthoni, P., Thiery, W., Laguë, M. M., Lawrence, D., and Lo, M.-H.: Global climate response to idealized deforestation in CMIP6 models, Biogeosciences, 17, 5615–5638, https://doi.org/10.5194/bg-17-5615-2020, 2020.

https://doi.org/10.5194/egusphere-2026-513
Preprint. Discussion started: 23 March 2026

Burton, C., Betts, R., Cardoso, M., Feldpausch, T. R., Harper, A., Jones, C. D., Kelley, D. I., Robertson, E., and Wiltshire, A.: Representation of fire, land-use change and vegetation dynamics in the Joint UK Land Environment Simulator vn4.9 (JULES), Geoscientific Model Development, 12, 179–193, https://doi.org/10.5194/gmd-12-179-2019, 2019.

Clark, D. B., Mercado, L. M., Sitch, S., Jones, C. D., Gedney, N., Best, M. J., Pryor, M., Rooney, G. G., Essery, R. L. H., Blyth, E., Boucher, O., Harding, R. J., Huntingford, C., and Cox, P. M.: The Joint UK Land Environment Simulator (JULES), model description – Part 2: Carbon fluxes and vegetation dynamics, Geoscientific Model Development, 4, 701–722, https://doi.org/10.5194/gmd-4-701-2011, 2011.

Collatz, G. J., Ribas-Carbo, M., and Berry, J. A.: Coupled Photosynthesis-Stomatal Conductance Model for Leaves of C4 Plants, Functional Plant Biology, 19, 519–538, https://doi.org/10.1071/pp9920519, 1992.

Cox, P. M.: Description of the TRIFFID dynamic global vegetation model, Tech. Rep. Technical Note 30, Met Office Hadley Centre, Exeter, UK, 2001.

Cui, J., Lian, X., Huntingford, C., Gimeno, L., Wang, T., Ding, J., He, M., Xu, H., Chen, A., Gentine, P., and Piao, S.: Global water availability boosted by vegetation-driven changes in atmospheric moisture transport, Nature Geoscience, 15, 982–988, https://doi.org/10.1038/s41561-022-01061-7, 2022.

Danabasoglu, G., Lamarque, J.-F., Bacmeister, J., Bailey, D. A., DuVivier, A. K., Edwards, J., Emmons, L. K., Fasullo, J., Garcia, R., Gettelman, A., Hannay, C., Holland, M. M., Large, W. G., Lauritzen, P. H., Lawrence, D. M., Lenaerts, J. T. M., Lindsay, K., Lipscomb, W. H., Mills, M. J., Neale, R., Oleson, K. W., Otto-Bliesner, B., Phillips, A. S., Sacks, W., Tilmes, S., van Kampenhout, L., Vertenstein, M., Bertini, A., Dennis, J., Deser, C., Fischer, C., Fox-Kemper, B., Kay, J. E., Kinnison, D., Kushner, P. J., Larson, V. E., Long, M. C., Mickelson, S., Moore, J. K., Nienhouse, E., Polvani, L., Rasch, P. J., and Strand, W. G.: The Community Earth System Model Version 2 (CESM2), Journal of Advances in Modeling Earth Systems, 12, e2019MS001 916, https://doi.org/10.1029/2019MS001916, 2020.

De Hertog, S. J., Havermann, F., Vanderkelen, I., Guo, S., Luo, F., Manola, I., Coumou, D., Davin, E. L., Duveiller, G., Lejeune, Q., Pongratz, J., Schleussner, C.-F., Seneviratne, S. I., and Thiery, W.: The biogeophysical effects of idealized land cover and land management changes in Earth system models, Earth System Dynamics, 14, 629–667, https://doi.org/10.5194/esd-14-629-2023, 2023.

Decharme, B.: Influence of runoff parameterization on continental hydrology: Comparison between the Noah and the ISBA land surface models, Journal of Geophysical Research: Atmospheres, 112, https://doi.org/10.1029/2007JD008463, 2007.

Devaraju, N., Bala, G., and Modak, A.: Effects of large-scale deforestation on precipitation in the monsoon regions: Remote versus local effects, Proceedings of the National Academy of Sciences, 112, 3257–3262, https://doi.org/10.1073/pnas.1423439112, 2015.

Di Vittorio, A. V., Chini, L. P., Bond-Lamberty, B., Mao, J., Shi, X., Truesdale, J., Craig, A., Calvin, K., Jones, A., Collins, W. D., Edmonds, J., Hurtt, G. C., Thornton, P., and Thomson, A.: From land use to land cover: restoring the afforestation signal in a coupled integrated assessment–earth system model and the implications for CMIP5 RCP simulations, Biogeosciences, 11, 6435–6450, https://doi.org/10.5194/bg-11-6435-2014, 2014.

Döscher, R., Acosta, M., Alessandri, A., Anthoni, P., Arsouze, T., Bergman, T., Bernardello, R., Boussetta, S., Caron, L.-P., Carver, G., Castrillo, M., Catalano, F., Cvijanovic, I., Davini, P., Dekker, E., Doblas-Reyes, F. J., Docquier, D., Echevarria, P., Fladrich, U., Fuentes-Franco, R., Gröger, M., v. Hardenberg, J., Hieronymus, J., Karami, M. P., Keskinen, J.-P., Koenigk, T., Makkonen, R., Massonnet, F., Ménégoz, M., Miller, P. A., Moreno-Chamarro, E., Nieradzik, L., van Noije, T., Nolan, P., O'Donnell, D., Ollinaho, P., van den Oord, G., Ortega, P., Prims, O. T., Ramos, A., Reerink, T., Rousset, C., Ruprich-Robert, Y., Le Sager, P., Schmith, T., Schrödner, R., Serva, F., Sicardi, V., Sloth Madsen, M., Smith, B., Tian, T., Tourigny, E., Uotila, P., Vancoppenolle, M., Wang, S., Wårlind, D., Willén, U., Wyser, K., Yang, S., Yepes-Arbós, X., and Zhang, Q.: The EC-Earth3 Earth system model for the Coupled Model Intercomparison Project 6, Geoscientific Model Development, 15, 2973–3020, https://doi.org/10.5194/gmd-15-2973-2022, 2022.

https://doi.org/10.5194/egusphere-2026-513
Preprint. Discussion started: 23 March 2026

Egerer, S., Lawrence, D. M., Lawrence, P. J., Argles, A., Arora, V., Barbu, A. L., Harman, I. N., Miller, P. A., Raddatz, T., Vuichard, N., Wårlind, D., Ziehn, T., and Pongratz, J.: Forestation in CMIP6: wide model spread in tree cover and land carbon uptake, Environmental Research Letters, 20, 054 033, https://doi.org/10.1088/1748-9326/adc93e, 2025.

Engel, F., Hoek van Dijke, A. J., Roebroek, C. T. J., and Benedict, I.: Can large-scale tree cover change negate climate change impacts on future water availability?, Hydrology and Earth System Sciences, 29, 1895–1918, https://doi.org/10.5194/hess-29-1895-2025, 2025.

Eyring, V., Bony, S., Meehl, G. A., Senior, C. A., Stevens, B., Stouffer, R. J., and Taylor, K. E.: Overview of the Coupled Model Intercomparison Project Phase 6 (CMIP6) experimental design and organization, Geoscientific Model Development, 9, 1937–1958, 2016.

Fahrenbach, N. L. S., Wills, R. C. J., and De Hertog, S. J.: Mechanistic insights into tropical circulation and hydroclimate responses to future forest cover change, Weather and Climate Dynamics, 6, 1461–1477, https://doi.org/10.5194/wcd-6-1461-2025, 2025.

Falkenmark, M.: Land–water linkages: a synopsis, in: Land and Water Integration and River Basin Management, Proceedings of the FAO Workshop, Rome, 31 January–2 February 1993, pp. 15–17, FAO, Rome, 1995.

Falkenmark, M. and Rockström, J.: The New Blue and Green Water Paradigm: Breaking New Ground for Water Resources Planning and Management, Journal of Water Resources Planning and Management, 132, 129–132, https://doi.org/10.1061/(ASCE)0733-9496(2006)132:3(129), 2006.

Farley, K. A., Jobbágy, E. G., and Jackson, R. B.: Effects of afforestation on water yield: a global synthesis with implications for policy, Global Change Biology, 11, 1565–1576, https://doi.org/10.1111/j.1365-2486.2005.01011.x, 2005.

Farquhar, G. D., von Caemmerer, S., and Berry, J. A.: A biochemical model of photosynthetic CO2 assimilation in leaves of C3 species, Planta, 149, 78–90, https://doi.org/10.1007/BF00386231, 1980.

Findell, K. L., Gentine, P., Lintner, B. R., and Kerr, C.: Probability of afternoon precipitation in eastern United States and Mexico enhanced by high evaporation, Nature Geoscience, 4, 434–439, https://doi.org/10.1038/ngeo1174, 2011.

Friedlingstein, P., O'Sullivan, M., Jones, M. W., Andrew, R. M., Bakker, D. C. E., Hauck, J., Landschützer, P., Le Quéré, C., Luijkx, I. T., Peters, G. P., Peters, W., Pongratz, J., Schwingshackl, C., Sitch, S., Canadell, J. G., Ciais, P., Jackson, R. B., Alin, S. R., Anthoni, P., Barbero, L., Bates, N. R., Becker, M., Bellouin, N., Decharme, B., Bopp, L., Brasika, I. B. M., Cadule, P., Chamberlain, M. A., Chandra, N., Chau, T.-T.-T., Chevallier, F., Chini, L. P., Cronin, M., Dou, X., Enyo, K., Evans, W., Falk, S., Feely, R. A., Feng, L., Ford, D. J., Gasser, T., Ghattas, J., Gkritzalis, T., Grassi, G., Gregor, L., Gruber, N., Gürses, O., Harris, I., Hefner, M., Heinke, J., Houghton, R. A., Hurtt, G. C., Iida, Y., Ilyina, T., Jacobson, A. R., Jain, A., Jarníková, T., Jersild, A., Jiang, F., Jin, Z., Joos, F., Kato, E., Keeling, R. F., Kennedy, D., Klein Goldewijk, K., Knauer, J., Korsbakken, J. I., Körtzinger, A., Lan, X., Lefèvre, N., Li, H., Liu, J., Liu, Z., Ma, L., Marland, G., Mayot, N., McGuire, P. C., McKinley, G. A., Meyer, G., Morgan, E. J., Munro, D. R., Nakaoka, S.-I., Niwa, Y., O'Brien, K. M., Olsen, A., Omar, A. M., Ono, T., Paulsen, M., Pierrot, D., Pocock, K., Poulter, B., Powis, C. M., Rehder, G., Resplandy, L., Robertson, E., Rödenbeck, C., Rosan, T. M., Schwinger, J., Séférian, R., Smallman, T. L., Smith, S. M., Sospedra-Alfonso, R., Sun, Q., Sutton, A. J., Sweeney, C., Takao, S., Tans, P. P., Tian, H., Tilbrook, B., Tsujino, H., Tubiello, F., van der Werf, G. R., van Ooijen, E., Wanninkhof, R., Watanabe, M., Wimart-Rousseau, C., Yang, D., Yang, X., Yuan, W., Yue, X., Zaehle, S., Zeng, J., and Zheng, B.: Global Carbon Budget 2023, Earth System Science Data, 15, 5301–5369, https://doi.org/10.5194/essd-15-5301-2023, 2023.

Fu, Z., Ciais, P., Wigneron, J.-P., Gentine, P., Feldman, A. F., Makowski, D., Viovy, N., Kemanian, A. R., Goll, D. S., Stoy, P. C., Prentice, I. C., Yakir, D., Liu, L., Ma, H., Li, X., Huang, Y., Yu, K., Zhu, P., Li, X., Zhu, Z., Lian, J., and Smith, W. K.: Global critical soil moisture thresholds of plant water stress, Nature Communications, 15, 4826, https://doi.org/10.1038/s41467-024-49244-7, 2024.

Fujimori, S., Hasegawa, T., Masui, T., Takahashi, K., Herran, D. S., Dai, H., Hijioka, Y., and Kainuma, M.: SSP3: AIM implementation of Shared Socioeconomic Pathways, Global Environmental Change, 42, 268–283, https://doi.org/10.1016/j.gloenvcha.2016.06.009, 2017.

https://doi.org/10.5194/egusphere-2026-513
Preprint. Discussion started: 23 March 2026

Gleeson, T., Wang-Erlandsson, L., Porkka, M., Zipper, S. C., Jaramillo, F., Gerten, D., Fetzer, I., Cornell, S. E., Piemontese, L., Gordon, L. J., Rockström, J., Oki, T., Sivapalan, M., Wada, Y., Brauman, K. A., Flörke, M., Bierkens, M. F. P., Lehner, B., Keys, P., Kummu, M., Wagener, T., Dadson, S., Troy, T. J., Steffen, W., Falkenmark, M., and Famiglietti, J. S.: Illuminating water cycle modifications and Earth system resilience in the Anthropocene, Water Resources Research, 56, e2019WR024 957, https://doi.org/10.1029/2019WR024957, 2020.

Guo, Q., Yoshida, N., Li, S., Nitta, T., Takeshima, A., Nitta, T., Onuma, Y., Satoh, Y., Suzuki, T., Takata, K., Yoshida, N., and Yoshimura, K.: Description of MATSIRO6, https://doi.org/10.15083/0002000181, 2021.

Hajima, T., Watanabe, M., Yamamoto, A., Tatebe, H., Noguchi, M. A., Abe, M., Ohgaito, R., Ito, A., Yamazaki, D., Okajima, H., Ito, A., Takata, K., Ogochi, K., Watanabe, S., and Kawamiya, M.: Development of the MIROC-ES2L Earth system model and the evaluation of biogeochemical processes and feedbacks, Geoscientific Model Development, 13, 2197–2244, https://doi.org/10.5194/gmd-13-2197-2020, 2020.

Heselschwerdt, S. P., Wagener, T., Wang-Erlandsson, L., Ukkola, A. M., Markonis, Y., Yang, Y., and Greve, P.: Large impact of extreme precipitation on projected blue-green water shares, EGUsphere, pp. 1–28, https://doi.org/10.5194/egusphere-2025-5896, 2025.

Hoek van Dijke, A. J., Herold, M., Mallick, K., Benedict, I., Machwitz, M., Schlerf, M., Pranindita, A., Theeuwen, J. J. E., Bastin, J.-F., and Teuling, A. J.: Shifts in regional water availability due to global tree restoration, Nature Geoscience, 15, 363–368, https://doi.org/10.1038/s41561-022-00935-0, 2022.

Hoekstra, A. Y.: Green-blue water accounting in a soil water balance, Advances in Water Resources, 129, 112–117, https://doi.org/10.1016/j.advwatres.2019.05.012, 2019.

Hurtt, G. C., Chini, L., Sahajpal, R., Frolking, S., Bodirsky, B. L., Calvin, K., Doelman, J. C., Fisk, J., Fujimori, S., Klein Goldewijk, K., Hasegawa, T., Havlik, P., Heinimann, A., Humpenöder, F., Jungclaus, J., Kaplan, J. O., Kennedy, J., Krisztin, T., Lawrence, D., Lawrence, P., Ma, L., Mertz, O., Pongratz, J., Popp, A., Poulter, B., Riahi, K., Shevliakova, E., Stehfest, E., Thornton, P., Tubiello, F. N., van Vuuren, D. P., and Zhang, X.: Harmonization of global land use change and management for the period 850–2100 (LUH2) for CMIP6, Geoscientific Model Development, 13, 5425–5464, https://doi.org/10.5194/gmd-13-5425-2020, 2020.

Ito, A. and Inatomi, M.: Use of a process-based model for assessing the methane budgets of global terrestrial ecosystems and evaluation of uncertainty, Biogeosciences, 9, 759–773, https://doi.org/10.5194/bg-9-759-2012, 2012.

Jackson, R. B., Jobbágy, E. G., Avissar, R., Roy, S. B., Barrett, D. J., Cook, C. W., Farley, K. A., le Maitre, D. C., McCarl, B. A., and Murray, B. C.: Trading Water for Carbon with Biological Carbon Sequestration, Science, 310, 1944–1947, https://doi.org/10.1126/science.1119282, 2005.

King, J. A., Weber, J., Lawrence, P., Roe, S., Swann, A. L. S., and Val Martin, M.: Global and regional hydrological impacts of global forest expansion, Biogeosciences, 21, 3883–3902, https://doi.org/10.5194/bg-21-3883-2024, 2024.

Koenker, R. and Hallock, K. F.: Quantile Regression, Journal of Economic Perspectives, 15, 143–156, https://doi.org/10.1257/jep.15.4.143, 2001.

Koven, C. D., Riley, W. J., Subin, Z. M., Tang, J. Y., Torn, M. S., Collins, W. D., Bonan, G. B., Lawrence, D. M., and Swenson, S. C.: The effect of vertically resolved soil biogeochemistry and alternate soil C and N models on C dynamics of CLM4, Biogeosciences, 10, 7109–7131, https://doi.org/10.5194/bg-10-7109-2013, 2013.

Laguë, M. M. and Swann, A. L. S.: Progressive Midlatitude Afforestation: Impacts on Clouds, Global Energy Transport, and Precipitation, Journal of Climate, 29, 5561–5573, https://doi.org/10.1175/JCLI-D-15-0748.1, 2016.

https://doi.org/10.5194/egusphere-2026-513
Preprint. Discussion started: 23 March 2026

Lawrence, D. M., Hurtt, G. C., Arneth, A., Brovkin, V., Calvin, K. V., Jones, A. D., Jones, C. D., Lawrence, P. J., de Noblet-Ducoudré, N., Pongratz, J., Seneviratne, S. I., and Shevliakova, E.: The Land Use Model Intercomparison Project (LUMIP) contribution to CMIP6: rationale and experimental design, Geoscientific Model Development, 9, 2973–2998, https://doi.org/10.5194/gmd-9-2973-2016, 2016.

Li, W., Zhang, Y., Shi, X., Zhou, W., Huang, A., Mu, M., Qiu, B., and Ji, J.: Development of Land Surface Model BCC_AVIM2.0 and Its Preliminary Performance in LS3MIP/CMIP6, Journal of Meteorological Research, 33, 851–869, https://doi.org/10.1007/s13351-019-9016-y, 2019.

Li, Y., Baker, J. C. A., Brando, P. M., Hoffman, F. M., Lawrence, D. M., Morton, D. C., Swann, A. L. S., Uribe, M. d. R., and Randerson, J. T.: Future increases in Amazonia water stress from CO2 physiology and deforestation, Nature Water, 1, 769–777, https://doi.org/10.1038/s44221-023-00128-y, 2023.

Loughran, T. F., Ziehn, T., Law, R., Canadell, J. G., Pongratz, J., Liddicoat, S., Hajima, T., Ito, A., Lawrence, D. M., and Arora, V. K.: Limited Mitigation Potential of Forestation Under a High Emissions Scenario: Results From Multi-Model and Single Model Ensembles, Journal of Geophysical Research: Biogeosciences, 128, e2023JG007 605, https://doi.org/10.1029/2023JG007605, 2023.

Lovato, T., Peano, D., Butenschön, M., Materia, S., Iovino, D., Scoccimarro, E., Fogli, P. G., Cherchi, A., Bellucci, A., Gualdi, S., Masina, S., and Navarra, A.: CMIP6 Simulations With the CMCC Earth System Model (CMCC-ESM2), Journal of Advances in Modeling Earth Systems, 14, e2021MS002 814, https://doi.org/10.1029/2021MS002814, 2022.

Ma, L., Hurtt, G. C., Chini, L. P., Sahajpal, R., Pongratz, J., Frolking, S., Stehfest, E., Klein Goldewijk, K., O'Leary, D., and Doelman, J. C.: Global rules for translating land-use change (LUH2) to land-cover change for CMIP6 using GLM2, Geoscientific Model Development, 13, 3203–3220, https://doi.org/10.5194/gmd-13-3203-2020, 2020.

Niu, G.-Y., Yang, Z.-L., Dickinson, R. E., and Gulden, L. E.: A simple TOPMODEL-based runoff parameterization (SIMTOP) for use in global climate models, Journal of Geophysical Research: Atmospheres, 110, https://doi.org/10.1029/2005JD006111, 2005.

Oleson, K. W., Lawrence, D. M., Bonan, G. B., Drewniak, B., Huang, M., Koven, C. D., Levis, S., Li, F., Riley, W. J., Subin, Z. M., Swenson, S. C., Thornton, P., Bozbiyik, A., Rosie, F., Heald, C. L., Kluzek, E., Lamarque, J.-F., Lawrence, P. J., Leung, L. R., Lipscomb, W., Muszala, S., Ricciuto, D. M., Sacks, W., Sun, Y., Tang, J., and Yang, Z.-L.: Technical description of version 4.5 of the Community Land Model (CLM), Technical Note NCAR/TN-503+STR, National Center for Atmospheric Research (NCAR), Boulder, CO, USA, 2013.

Orth, R. and Destouni, G.: Drought reduces blue-water fluxes more strongly than green-water fluxes in Europe, Nature Communications, 9, 3602, 2018.

Pitman, A. J., de Noblet-Ducoudré, N., Cruz, F. T., Davin, E. L., Bonan, G. B., Brovkin, V., Claussen, M., Delire, C., Ganzeveld, L., Gayler, V., van den Hurk, B. J. J. M., Lawrence, P. J., van der Molen, M. K., Müller, C., Reick, C. H., Seneviratne, S. I., Strengers, B. J., and Voldoire, A.: Uncertainties in climate responses to past land cover change: First results from the LUCID intercomparison study, Geophysical Research Letters, 36, https://doi.org/10.1029/2009GL039076, 2009.

Pongratz, J., Schwingshackl, C., Bultan, S., Obermeier, W., Havermann, F., and Guo, S.: Land Use Effects on Climate: Current State, Recent Progress, and Emerging Topics, Current Climate Change Reports, 7, 99–120, https://doi.org/10.1007/s40641-021-00178-y, 2021.

Portmann, R., Beyerle, U., Davin, E., Fischer, E. M., De Hertog, S., and Schemm, S.: Global forestation and deforestation affect remote climate via adjusted atmosphere and ocean circulation, Nature Communications, 13, 5569, https://doi.org/10.1038/s41467-022-33279-9, 2022.

Riahi, K., Van Vuuren, D. P., Kriegler, E., Edmonds, J., O'Neill, B. C., Fujimori, S., Bauer, N., Calvin, K., Dellink, R., Fricko, O., Lutz, W., Popp, A., Cuaresma, J. C., Kc, S., Leimbach, M., Jiang, L., Kram, T., Rao, S., Emmerling, J., Ebi, K., Hasegawa, T., Havlik, P., Humpenöder, F., Da Silva, L. A., Smith, S., Stehfest, E., Bosetti, V., Eom, J., Gernaat, D., Masui, T., Rogelj, J., Strefler, J., Drouet,

https://doi.org/10.5194/egusphere-2026-513
Preprint. Discussion started: 23 March 2026

L., Krey, V., Luderer, G., Harmsen, M., Takahashi, K., Baumstark, L., Doelman, J. C., Kainuma, M., Klimont, Z., Marangoni, G., Lotze-Campen, H., Obersteiner, M., Tabeau, A., and Tavoni, M.: The Shared Socioeconomic Pathways and their energy, land use, and greenhouse gas emissions implications: An overview, Global Environmental Change, 42, 153–168, https://doi.org/10.1016/j.gloenvcha.2016.05.009, 2017.

Ricciardi, L., D'Odorico, P., Galli, N., Chiarelli, D. D., and Rulli, M. C.: Hydrological implications of large-scale afforestation in tropical biomes for climate change mitigation, Philosophical Transactions of the Royal Society B: Biological Sciences, 377, 20210391, https://doi.org/10.1098/rstb.2021.0391, 2022.

Rockström, J. and Gordon, L.: Assessment of green water flows to sustain major biomes of the world: Implications for future ecohydrological landscape management, Physics and Chemistry of the Earth, Part B: Hydrology, Oceans and Atmosphere, 26, 843–851, https://doi.org/10.1016/S1464-1909(01)00096-X, 2001.

Santos, J. F., Schickhoff, U., ul Hasson, S., and Böhner, J.: Biogeophysical Effects of Land-Use and Land-Cover Changes in South Asia: An Analysis of CMIP6 Models, Land, 12, 880, https://doi.org/10.3390/land12040880, 2023.

Sellar, A. A., Jones, C. G., Mulcahy, J. P., Tang, Y., Yool, A., Wiltshire, A., O'Connor, F. M., Stringer, M., Hill, R., Palmieri, J., Woodward, S., de Mora, L., Kuhlbrodt, T., Rumbold, S. T., Kelley, D. I., Ellis, R., Johnson, C. E., Walton, J., Abraham, N. L., Andrews, M. B., Andrews, T., Archibald, A. T., Berthou, S., Burke, E., Blockley, E., Carslaw, K., Dalvi, M., Edwards, J., Folberth, G. A., Gedney, N., Griffiths, P. T., Harper, A. B., Hendry, M. A., Hewitt, A. J., Johnson, B., Jones, A., Jones, C. D., Keeble, J., Liddicoat, S., Morgenstern, O., Parker, R. J., Predoi, V., Robertson, E., Siahaan, A., Smith, R. S., Swaminathan, R., Woodhouse, M. T., Zeng, G., and Zerroukat, M.: UKESM1: Description and Evaluation of the U.K. Earth System Model, Journal of Advances in Modeling Earth Systems, 11, 4513–4558, https://doi.org/10.1029/2019MS001739, 2019.

Sellers, P. J., Randall, D. A., Collatz, G. J., Berry, J. A., Field, C. B., Dazlich, D. A., Zhang, C., Collelo, G. D., and Bounoua, L.: A Revised Land Surface Parameterization (SiB2) for Atmospheric GCMS. Part I: Model Formulation, Journal of Climate, 9, 676–705, https://doi.org/10.1175/1520-0442(1996)009<0676:ARLSPF>2.0.CO;2, 1996.

Spracklen, D. V., Arnold, S. R., and Taylor, C. M.: Observations of increased tropical rainfall preceded by air passage over forests, Nature, 489, 282–285, https://doi.org/10.1038/nature11390, 2012.

Staal, A., Tuinenburg, O. A., Bosmans, J. H. C., Holmgren, M., van Nes, E. H., Scheffer, M., Zemp, D. C., and Dekker, S. C.: Forest-rainfall cascades buffer against drought across the Amazon, Nature Climate Change, 8, 539–543, https://doi.org/10.1038/s41558-018-0177-y, 2018.

Staal, A., Meijer, P., Nyasulu, M. K., Tuinenburg, O. A., and Dekker, S. C.: Global terrestrial moisture recycling in Shared Socioeconomic Pathways, Earth System Dynamics, 16, 215–238, https://doi.org/10.5194/esd-16-215-2025, 2025.

Swann, A. L. S., Fung, I. Y., and Chiang, J. C. H.: Mid-latitude afforestation shifts general circulation and tropical precipitation, Proceedings of the National Academy of Sciences, 109, 712–716, https://doi.org/10.1073/pnas.1116706108, 2012.

Swart, N. C., Cole, J. N. S., Kharin, V. V., Lazare, M., Scinocca, J. F., Gillett, N. P., Anstey, J., Arora, V., Christian, J. R., Hanna, S., Jiao, Y., Lee, W. G., Majaess, F., Saenko, O. A., Seiler, C., Seinen, C., Shao, A., Sigmond, M., Solheim, L., von Salzen, K., Yang, D., and Winter, B.: The Canadian Earth System Model version 5 (CanESM5.0.3), Geoscientific Model Development, 12, 4823–4873, https://doi.org/10.5194/gmd-12-4823-2019, 2019.

Séférian, R., Nabat, P., Michou, M., Saint-Martin, D., Voldoire, A., Colin, J., Decharme, B., Delire, C., Berthet, S., Chevallier, M., Sénési, S., Franchisteguy, L., Vial, J., Mallet, M., Joetzjer, E., Geoffroy, O., Guérémy, J.-F., Moine, M.-P., Msadek, R., Ribes, A., Rocher, M., Roehrig, R., Salas-y Mélia, D., Sanchez, E., Terray, L., Valcke, S., Waldman, R., Aumont, O., Bopp, L., Deshayes, J., Éthé, C., and

https://doi.org/10.5194/egusphere-2026-513
Preprint. Discussion started: 23 March 2026

Madec, G.: Evaluation of CNRM Earth System Model, CNRM-ESM2-1: Role of Earth System Processes in Present-Day and Future Climate, Journal of Advances in Modeling Earth Systems, 11, 4182–4227, https://doi.org/10.1029/2019MS001791, 2019.

Takata, K., Emori, S., and Watanabe, T.: Development of the minimal advanced treatments of surface interaction and runoff, Global and Planetary Change, 38, 209–222, https://doi.org/10.1016/S0921-8181(03)00030-4, 2003.

te Wierik, S. A., Cammeraat, E. L. H., Gupta, J., and Artzy-Randrup, Y. A.: Reviewing the Impact of Land Use and Land-Use Change on Moisture Recycling and Precipitation Patterns, Water Resources Research, 57, e2020WR029 234, https://doi.org/10.1029/2020WR029234, 2021.

Tuinenburg, O. A., Theeuwen, J. J. E., and Staal, A.: High-resolution global atmospheric moisture connections from evaporation to precipitation, Earth System Science Data, 12, 3177–3188, https://doi.org/10.5194/essd-12-3177-2020, 2020.

van der Ent, R. J., Savenije, H. H. G., Schaefli, B., and Steele-Dunne, S. C.: Origin and fate of atmospheric moisture over continents, Water Resources Research, 46, https://doi.org/10.1029/2010WR009127, 2010.

Wang-Erlandsson, L., Fetzer, I., Keys, P. W., van der Ent, R. J., Savenije, H. H. G., and Gordon, L. J.: Remote land use impacts on river flows through atmospheric teleconnections, Hydrology and Earth System Sciences, 22, 4311–4328, https://doi.org/10.5194/hess-22-4311-2018, 2018.

Wu, T., Lu, Y., Fang, Y., Xin, X., Li, L., Li, W., Jie, W., Zhang, J., Liu, Y., Zhang, L., Zhang, F., Zhang, Y., Wu, F., Li, J., Chu, M., Wang, Z., Shi, X., Liu, X., Wei, M., Huang, A., Zhang, Y., and Liu, X.: The Beijing Climate Center Climate System Model (BCC-CSM): the main progress from CMIP5 to CMIP6, Geoscientific Model Development, 12, 1573–1600, https://doi.org/10.5194/gmd-12-1573-2019, 2019.